Journal of the Meteorological Society of Japan

EARLY ONLINE RELEASE

The DOI for this manuscript is

DOI:10.2151/jmsj.2020-059

J-STAGE Advance published date: August 3rd 2020

The final manuscript after publication will replace the preliminary version at the above DOI once it is available.

Marine Low Clouds and Their Parameterization in Climate Models

Hideaki KAWAI[1]

Meteorological Research Institute
Tsukuba, Japan

and

Shoichi SHIGE

Graduate School of Science
Kyoto University, Kyoto, Japan

January 24, 2020

----

1) Corresponding author: Hideaki Kawai, Meteorological Research Institute, 1-1 Nagamine, Tsukuba, Ibaraki, 305-0052, JAPAN.
Email: h-kawai@mri-jma.go.jp
Tel: +81-29-853-8666
Fax: +81-29-855-6936

Abstract

This review paper aims to provide readers with a broad range of meteorological backgrounds with basic information on marine low clouds and the concept of their parameterizations used in global climate models. The first part of the paper presents basic information on marine low clouds and their importance in climate simulations in a comprehensible way. It covers the global distribution and important physical processes related to the clouds, typical examples of observational and modeling studies of such clouds, and the considerable importance of changes in low cloud for climate simulations. In the latter half of the paper, the concept of cloud parameterizations that determine cloud fraction and cloud water content in global climate models, which is sometimes called cloud "macrophysics", is introduced. In the parameterizations, the key element is how to assume or determine the inhomogeneity of water vapor and cloud water content in model grid boxes whose size is several tens to several hundreds of kilometers. Challenges related to cloud representation in such models that must be tackled in the next couple of decades are discussed.

Keywords low cloud; climate model; cloud parameterization; climate change

1. Introduction

Marine low clouds (MLCs), or marine boundary layer clouds (MBLCs), are low-level clouds prevalent over the ocean. Optically thick MLCs typically prevail over oceans with low sea surface temperature (SST) and high lower-tropospheric stability (e.g., Klein and Hartmann 1993). Although they are not associated with heavy rain or strong wind, MLCs are important for the global radiation budget because of their large shortwave radiative effects. Recent studies have shown that uncertainties in predicted temperature increases in global warming simulations can be mainly attributed to the representation of MLCs in global climate models (GCMs) (e.g., Stephens 2005, Bony and Dufresne 2005, Bony et al. 2006, Boucher et al. 2013, Zelinka et al. 2020).

The purpose of this review paper is to provide fundamental knowledge of low clouds and their parameterizations in GCMs to readers with a wide variety of meteorological backgrounds, rather than providing experts in this area with a summary of recent related studies. An introduction to marine low clouds, including their global distribution and important physical processes related to the clouds, is given in Section 2. Some observational and modeling studies of these clouds are introduced in Section 3. The importance of low cloud change on climate simulations is then introduced in Section 4.

For climate simulations, we need global atmospheric models coupled with ocean models. However, because the model grid boxes are generally several tens to several hundreds of kilometers in size, the models need a cloud parameterization that represents the subgrid-scale inhomogeneity of clouds and humidity (and temperature). This is often termed cloud macrophysics and the main purpose is to determine the cloud fraction and cloud water content of the model grid cells. The latter half of this paper provides a basic review of such parameterizations and discussions of some difficulties related to the representation of clouds in GCMs (Section 5). Although turbulence schemes, schemes for shallow convection, and cloud microphysics also affect the representation of marine low clouds in GCMs, they are beyond the scope of this review paper. In Section 6, other topics that exert significant influences on climate simulations are briefly introduced, including the difficulties and uncertainty in representing cloud phase and aerosol–cloud interactions in GCMs. Sections 5 and 6 would be useful for those who wish to tackle cloud parameterizations in GCMs or those who are not modelers but who analyze cloud data from climate simulations such as the Coupled Model Intercomparison Project (CMIP) (Meehl et al. 2000).

2. Brief Overview of Marine Low Clouds

The characteristics of MLCs are completely different from mid-level clouds or high-level clouds. Typically, low-level approximately refers to 700 hPa or lower, high-level to 400 hPa or higher, and mid-level to the intermediate heights (e.g., Rossow and Schiffer 1999). Mid- and high-level clouds are often associated with deep convection or the warm front of extra-tropical cyclones, where updrafts play an important role in condensing water vapor into clouds. On the other hand, optically thick MLCs typically form under high pressure systems, accompanied by the subsidence of air, for example under subtropical high pressure systems and the Okhotsk high pressure system. While mid- and high-level clouds climatologically tend to develop over areas with high SST, MLCs typically occur over the ocean where SST is low. In contrast to mid- and high-level clouds, which are often associated with precipitation, MLCs typically generate either no precipitation or only drizzle. Therefore, the roles of mid- and high-level clouds and MLCs in the Earth's atmosphere are entirely different. While deep clouds, which are accompanied by precipitation, heat or cool the surrounding atmosphere through latent heat release or evaporative cooling (e.g., Houze 1982, 2004, Shige et al. 2004, Sui et al. 2020), MLCs, especially stratus and stratocumulus, mainly exert an influence through the radiative effect, which is discussed in Section 2.2.

2.1 Global Distribution of MLCs

An image of MLCs over the subtropical north eastern Pacific (an area renowned for the frequent occurrence of MLCs and a clear transition of MLC regimes) is shown in Fig. 1. The visible image was taken by the Moderate Resolution Imaging Spectroradiometer (MODIS). Flat and homogeneous clouds off the coast of California are stratus. A transition of MLC regimes from stratus to stratocumulus, which has a clear meso-scale structure (Wood

2012), is observed in a west-southwestward direction. Farther west-southwestward, the MLC regime eventually changes from stratocumulus to cumulus, where cloud amount is much smaller than in areas dominated by stratus and stratocumulus; note that cloud amount or cloud cover is defined as the proportion of cloud covering an area. As clearly shown in Fig. 1, MLCs such as marine stratus and stratocumulus are characterized by high albedo.

Such optically thick MLCs generally prevail over the subtropics and parts of the tropics off the west coast of continents. Klein and Hartmann (1993) reported the global distribution of low stratiform cloud, which consists of stratus, stratocumulus, and sky-obscuring fog (Fig. 2). It is clear from the figure that boundary layer stratiform cloud amount is very large over the subtropical oceans off California, Peru, Namibia, and Mauritania. This study also found that Lower Tropospheric Stability (LTS), defined as the difference in potential temperature between 700 hPa and the surface, has a high correlation with boundary layer stratiform cloud amount and the global distribution of LTS corresponds closely to that of stratiform clouds. High stability over subtropical oceans off the west coast of continents is attributed to the fact that SST is low in those areas compared with other oceans at similar latitudes, although air temperature at 700 hPa is approximately uniform zonally (Fig. 3). The low SST is caused by horizontal cold advection from higher latitudes driven by subtropical gyre with the eastern boundary current (e.g., Colling 2001). Coastal upwelling of cold water also contributes to the low SST, especially near the coast. The physical mechanism for the high correlation between low cloud amount and stability is explained in Section 2.3.

2.2 Importance of MLCs in Climate and Weather

MLCs, including stratus and stratocumulus, are one of the most important cloud contributors to the global radiation budget because of their large shortwave radiative effects (e.g., Klein and Hartmann 1993). MLCs in the subtropics are especially important because solar insolation is relatively large in these regions compared with the mid or high latitudes. MLCs exert a significant control on global average temperature because of their significant influence on global albedo.

However, a realistic representation of marine stratocumulus clouds off the west coast of continents in global climate models (GCMs) has been a major issue in climate modeling for a long time (e.g., Duynkerke and Teixeira 2001, Siebesma et al. 2004). Current GCMs still have some deficiencies in representing subtropical marine stratocumulus clouds off the west coast of continents compared with observations (e.g., Nam et al. 2012, Caldwell et al. 2013, Su et al. 2013, Koshiro et al. 2018). Lauer and Hamilton (2013) showed that total cloud cover simulated in CMIP3 and CMIP5 multi-models is significantly underestimated over subtropical stratocumulus regions and there are large biases in shortwave cloud radiative effect over these regions (Fig. 4); these biases are astonishingly similar in the CMIP3 and CMIP5 multi-model means. Overestimates of SST of ~5 K off the west coast of continents are possible in ocean–atmosphere coupled models partly due to the poor representation of marine stratocumulus over these areas (e.g., Ma et al. 1996, Duynkerke and Teixeira 2001).

In fact, there are two kinds of importance associated with MLCs from a climate perspective. One is related to the representation of the present climate system as described above. The SST bias over areas with frequent MLC cover is a serious problem not just because it affects local SST. It can deteriorate the representation of the ocean general circulation, because, for instance, strong stabilization of the ocean occurs over areas with coastal upwelling. This would exert a major influence on the representation of the global climate system. The other importance associated with MLCs is related to climate change simulations. This issue, which is a hot topic whose importance has become evident since the 2000s, is explained in detail in Section 4.

Although they do not bring heavy rain or strong wind, MLCs are important not only for global climate systems but also for local and short-lived phenomena. A typical phenomenon that occurs in and around Japan is the Yamase cloud event in which MLCs accompany the Yamase winds (e.g., Kodama 1997, Kodama et al. 2009, Koseki et al. 2012, Shimada et al. 2014). When the Okhotsk high pressure system appears in summer, it causes northeasterly winds along the Pacific coast of the Tohoku region. Stratocumulus is formed off Tohoku under northeasterly winds (e.g., Shimada and Iwasaki 2015) and is continually advected over coastal areas (Fig. 5; e.g., Eguchi et al. 2014). The temperature in the area decreases dramatically due to the blocking of solar insolation in addition to cool air advection from the ocean. Until a few hundred years ago, large numbers of people even starved to death because of poor crop harvests caused by low temperatures. However, MLCs related to Yamase are also difficult to reproduce in atmospheric models, including numerical weather prediction (NWP) models.

In the next section, the reasons for the difficulty in reproducing MLCs realistically in atmospheric models are explained.

2.3 Mechanisms for the Formation and Maintenance of MLCs

While condensation due to the upward motion of an air mass is a primary factor in producing mid- and high-level clouds, MLCs are formed and maintained by a subtle balance between complicated physical processes (e.g., Duynkerke and Teixeira 2001, Wood 2012). Figure 6 shows a schematic diagram (modified from fig. 2 in de Roode and Duynkerke 1997) of the complicated physical processes that affect MLCs. For instance, the right edge of the figure might correspond to an area adjacent to California (Peru) where SST is lower, and the left edge to an area near Hawaii (far west of Peru) where SST is higher.

Subtropical high pressure systems over subtropical oceans are accompanied by subsidence in the free atmosphere. Subsidence generates a temperature inversion at the top of the boundary layer, which is very strong when SST is relatively low (near the right edge of Fig. 6). Stability is extremely high at the inversion layer, and the inversion prevents water vapor from escaping into the free atmosphere. Therefore, water vapor is confined in the boundary layer and condenses into clouds. Because stratus and stratocumulus clouds have high optical thickness and strong cloud top cooling, longwave radiative cooling plays an important role in developing and maintaining the cloud layer. The strong cloud top cooling destabilizes the boundary layer just below the inversion, promotes water vapor transport from the sea surface, and maintains the well-mixed layer and cloud layer. It can even strengthen the temperature inversion just above the cloud top.

The temperature inversion is weaker in areas where SST is higher by several degrees. Cloud top entrainment occurs in these areas, which is the process of taking dry and warm air into the mixed layer from the free atmosphere. Figure 7 shows a schematic illustration of cloud top entrainment (Randall 1980, Yamaguchi and Randall 2008). When a dry and warm air parcel enters the cloud layer from the free atmosphere, cloud water evaporates into the dry parcel and the temperature of the parcel is lowered. If the decrease of temperature is large enough to overcome the temperature gap (inversion) at the top of the cloud layer, the parcel can have negative buoyancy. In this case, dry and warm air can continuously intrude into the mixed layer. A weaker temperature inversion and/or larger gap of humidity at the cloud top are more favorable for cloud top entrainment. Drying of the mixed layer due to cloud top entrainment contributes to the break-up of the cloud layer (Deardorff 1980, Randall 1980). The cloud top entrainment and the role have been discussed based on observational or modeling studies by many researchers since the concept was proposed (e.g., Kuo and Schubert 1988, Betts and Boers 1990, MacVean and Mason 1990, MacVean 1993, Yamaguchi and Randall 2008, Lock 2009, Noda et al. 2013). In addition, higher SST causes shallow convection, which is observed as cumulus (e.g., Chung et al. 2012). Shallow convection forms a decoupled layer above the lifting condensation level that suppresses upward turbulent transport of water vapor to an upper part of a boundary layer (e.g., Sandu and Stevens 2011, de Roode et al. 2016), and they vent water vapor in the boundary layer to the free atmosphere (e.g., Stull 1988). Active shallow convection is more efficient at suppressing optically thick stratocumulus occurrence when SST is higher.

Thus, stratus and stratocumulus prevail in subtropical oceans adjacent to the west coast of continents, gradually break up westward, and disappear far from these landmasses (see Fig. 1). The cloud regimes change from solid stratus to stratocumulus to closed-cell convection, open-cell convection, and then scattered cumulus as SST increases with increasing distance from the coast. As explained above, the temperature inversion is an important factor controlling MLCs. The high correlation between low cloud amount and LTS (Section 2.1) is attributed to the high correlation between low cloud amount and temperature inversion strength, because there must be a correlation between LTS and temperature inversion strength. Wood and Bretherton (2006) modified LTS and developed a more sophisticated index, estimated inversion strength (EIS), which estimates the temperature inversion strength at the top of a mixed layer from LTS, assuming a moist adiabatic lapse rate in a free atmosphere. They showed that the correlation of low cloud amount with EIS is even higher than with LTS. Subsequently, Kawai et al. (2017) developed an index for low cloud amount, the estimated cloud-top entrainment index (ECTEI), which is a modification of EIS that considers the effect of cloud top entrainment. Figure 8 shows the relationships between low cloud amount and the stability indexes, LTS, EIS, and ECTEI. It shows that ECTEI has the best correlation with low cloud amount among the three indices, although EIS also has a high correlation.

There are clear diurnal variations in cloud amount and the liquid water path of stratus and stratocumulus, which reach a maximum in the early morning and a minimum in the early afternoon (e.g., Blaskovic et al. 1991, Albrecht et al. 1995, Rozendaal et al. 1995, Duynkerke and Teixeira 2001, de Szoeke et al. 2012, Burleyson et al. 2013); an example is shown in Fig. 9 below. During the daytime, solar insolation heats the cloud layer. Shortwave heating reduces net radiative cooling and weakens water vapor transport. In addition, shortwave radiation penetrates the cloud layer to some extent and heats the inside of the cloud layer, while longwave cooling only occurs several tens of meters from the cloud top. The difference in the heating and cooling heights causes decoupling of the mixed layer and prevents water vapor transport (e.g., Betts 1990, Blaskovic et al. 1991). The interactions of the related physical processes are even more complicated. For example, condensation of water vapor heats the inside of the cloud layer, longwave radiation from the sea surface heats the cloud base, and evaporation of drizzle cools the air below the cloud base. All of these processes affect the vertical profile of the cloud-topped boundary layer. Various physical processes that control MLCs and their complicated interactions are discussed in more detail in some review papers (e.g., Wood 2012, Nuijens and Siebesma 2019).

However, despite this complexity, the vertical resolution of GCMs is fairly low, and the thickness of model layers around the top of a mixed layer or cloud top of MLCs is 200–300 m, while the observed thickness of MLCs can be as small as 50 m during the daytime (Betts 1990, Duynkerke and Teixeira 2001). The lack of vertical resolution in GCMs is one of the major causes of the difficulty in reproducing MLCs, and the complicated physical interactions related to MLCs are extremely difficult to represent appropriately in current GCMs.

3. Observational and Modeling Studies

There are two methods for investigating MLCs. One is to obtain information from observational data, such as shipboard observations, satellite data, and field campaign data (including aircraft data). Another is to use models, including cloud resolving models (CRMs) and large eddy simulation (LES) models.

3.1 Observational Studies

Shipboard observations (e.g., Warren et al. 1988, Hahn and Warren 2009; Eastman et al. 2011) have been used to reveal the global distribution of MLCs. Although data are obtained from visual observation, and are consequently subjective to some extent, the advantages are large areal coverage (almost global), a long history (>50 years), and the fact that observations are made from below the cloud base. One of the most renowned observational studies is that of Klein and Hartmann (1993) (see Section 2.1). Subsequently, Norris (1998a, b) and Norris and Klein (2000) investigated the global distribution and the characteristics of each MLC regime using shipboard observational data.

Satellite data have also been used for studies of MLCs. The International Satellite Cloud Climatology Project (ISCCP) (e.g., Rossow and Schiffer 1999) is a dataset obtained from satellites that is frequently used for global studies related to clouds. Clouds are classified into cloud regimes, such as stratus, stratocumulus, cumulus, cirrus, and cumulonimbus, using infrared and visible channel data from geostationary satellites. For example, controlling factors for MLCs were investigated using satellite data including ISCCP data, and the sensitivities of MLCs to meteorological parameters including EIS, SST, subsidence, and surface temperature advections were revealed (e.g., Myers and Norris 2013, Myers and Norris 2015, Myers and Norris 2016, Qu et al. 2015, Seethala et al. 2015). However, though there are many advantages in using data from geostationary satellites, including the broad spatial area, high frequency (better than every three hours), and homogeneity of the observations, estimates of the cloud top height based on infrared data have a large uncertainty (Garay et al. 2008).

Several field campaigns have been carried out to reveal the detailed characteristics of MLCs (see Table 1), and the findings of these studies have resulted in a better understanding of the structures of MLCs and related processes. FIRE (First ISCCP Regional Experiment) was a field campaign undertaken in June and July 1987 to examine Californian coastal stratocumulus (Albrecht et al. 1988). ASTEX (the Atlantic Stratocumulus Transition Experiment) studied stratocumulus and subtropical trade cumulus over the northeast Atlantic Ocean during June 1992 (Albrecht et al. 1995). The EPIC (East Pacific Investigation of Climate) field campaign for stratocumulus off Peru was conducted in September and October of 2001 (Bretherton et al. 2004b). VOCALS-REx [the Variability of American monsoon systems (VAMOS) Ocean–Cloud–Atmosphere–Land Study Regional Experiment] was performed in October and November of 2008 to examine stratocumulus off Peru (Wood et al. 2011, Bretherton et al. 2010). A field campaign EUREC^{4}A (Elucidate the Couplings Between Clouds, Convection and Circulation) was conducted over the tropical Atlantic Ocean in January and February 2020 to investigate the relationships between trade cumulus and the large-scale environment (Bony et al. 2017). These field campaigns used various observational methods, including ceilometers, radiosondes, sodar, and aircraft, to observe the vertical structure of MLCs in detail, including cloud top and base heights, the liquid water path, and their diurnal variations. For instance, diurnal variations in liquid water path and cloud-top and cloud-base heights observed in the field campaign FIRE during July 1987 are shown in Fig. 9 (Blaskovic et al. 1991). Clear diurnal variation in liquid water path is observed, which reaches a maximum in the early morning and a minimum in the afternoon, as discussed in Section 2.3. The diurnal variation in cloud depth (the difference between cloud top and cloud base heights) is also captured, showing a minimum in the afternoon.

3.2 Modeling Studies

CRMs have been used in the past to understand the detailed characteristics of MLCs and the interactions of the related physical processes. LESs have been used more recently (e.g., Noda and Nakamura 2008), and have typical resolutions of 25–50 m horizontally and 5–10 m vertically. The advantage of using these models is that all variables, including cloud water content, temperature, and humidity, can be obtained completely and analyzed in detail. Another advantage is that many sensitivity tests can be conducted to understand the mechanisms of interactions between a variety of physical processes. For instance, Yamaguchi and Randall (2008) investigated cloud top entrainment for a cloud-topped mixed layer in detail using LES, and revealed the contributions to cloud formation and dissipation of the temperature inversion and humidity gap at the cloud top, longwave radiative cooling, and the surface latent heat flux. Noda et al. (2014) investigated responses of marine stratocumulus to various large-scale factors using LES, and concluded that gaps of humidity and temperature at the top of a boundary layer are the most dominant factors that control stratocumulus. Lock (2009) investigated factors that influence the cloud cover of shallow cumulus clouds using LES and found that the cloud-top entrainment parameter has a high correlation with cloud cover. Several intercomparison studies have evaluated the representation of MLCs in LESs. For instance, de Roode et al. (2016) showed that six LESs produced consistent simulations of the stratocumulus–cumulus transitions based on four different cases, including an example from the ASTEX field campaign. On the other hand, Sato et al. (2015) reported that the different microphysics schemes in an LES model cause significant differences in simulations of shallow cumulus. Furthermore, it has been shown that cloud cover of stratocumulus (Matheou and Teixeira 2019) and shallow cumulus (Sato et al. 2018b) simulated by LES does not converge until the vertical and horizontal resolutions of the model reach 5 m and about 10 m, respectively.

4. Climate Change Studies and MLCs

4.1 Uncertainty in Climate Change

Future climate change is one of the most important topics for climate and meteorological studies. However, there is a wide spread in predicted increases in surface temperature in global warming simulations by various climate models, and this spread has not narrowed even in recent years (e.g., Flato et al. 2013). It is widely recognized that a major part of this spread arises from large variations in cloud feedback (e.g., Soden and Held 2006, Soden et al. 2008). The term 'cloud feedback' is defined as a change in the radiative effects of clouds in response to an external climate perturbation, such as increased CO_2 [see Bony et al. (2006) for a more formal definition]. This feedback refers to the extent that changes in clouds amplify or dampen a change in surface air temperature caused directly by external forcing.

A substantial part of the spread in cloud feedback can be attributed to variability in predictions of low clouds, which have a large shortwave radiative effect (e.g., Stephens 2005, Bony et al. 2006, Zelinka et al. 2012a, 2012b, 2013, 2020). Generally speaking, increases (decreases) in low cloud cover or cloud optical thickness in future climates lead to decreases (increases) in solar insolation reaching the surface, thereby mitigating (enhancing) the temperature increase. Figure 10 shows estimates of surface temperature increase under doubled CO_2 concentrations from a number of models that participated in the CMIP. It also shows changes in low clouds for two models that fall at either end of the projected warming range (Stephens 2005). The Atmospheric Model version 2 (AM2) from the Geophysical Fluid Dynamics Laboratory (GFDL) and the National Center for Atmospheric Research (NCAR) Community Atmosphere Model (CAM) 2.0 have climate sensitivities of more than 4.5 K and less than 2 K, respectively. The difference in changes in low-level cloud amount in these two models is significant. A version of AM2 shows a strong decrease in subtropical low cloud, leading to albedo decreases and a positive cloud feedback, while CAM2.0 shows an increase in the low-level cloud amount and a negative feedback (Bretherton et al. 2004a). Note that positive (negative) cloud feedback corresponds to a change in cloud that amplifies (dampens) the change in surface air temperature due to external forcing.

Bony and Dufresne (2005) and Bony et al. (2006) divided coupled ocean–atmosphere GCMs participating in the Intergovernmental Panel on Climate Change (IPCC) Fourth Assessment Report (AR4) into two groups: those with positive cloud feedbacks over the tropics and those with negative feedbacks. They found that differences in the two groups are caused mainly by cloud regimes that form under strong subsidence, and that shortwave cloud radiative effect (CRE) rather than longwave CRE is responsible for the difference (Fig. 11). This means that changes in low cloud regimes, which have high albedo, have a dominant control on cloud feedback. This result is related to the fact that changes in low cloud regimes have a large impact on the net CRE due to the large shortwave radiative effect and small longwave CRE. On the other hand, changes in deep cloud regimes have a small impact on net CRE because an increase (decrease) in deep cloud amount causes more (less) reflection of solar radiation and comparably more (less) absorption of infrared emission from the surface. This corresponds to a negative (positive) impact on shortwave CRE and a positive (negative) impact on longwave CRE so that the effects almost cancel each other out (e.g., Zelinka et al. 2012a, 2013). Consequently, changes in deep cloud regimes do not have a large influence on cloud feedback. Although thin cirrus clouds have weak positive net CRE due to larger longwave CRE (positive) than shortwave CRE (negative), actual contribution of thin clouds to cloud feedback is not dominant (e.g., Zelinka et al. 2012a, 2013). More recently, it has also been confirmed that the spread of low cloud feedback dominantly contributes to the spread of net total cloud feedback based on simulation results using CMIP5 multi-models (Zelinka et al. 2013) and CMIP6 multi-models (Zelinka et al. 2020).

Therefore, to obtain reliable cloud feedback for low clouds and narrow the spread in the predicted increases in surface temperature, MLCs must be represented accurately in GCMs. The interactions of physical processes related to MLCs should be represented as well as possible, although it will not be easily achieved, as discussed in Section 2.3. Unfortunately, LESs cannot be used for global climate simulations due to limitations on computer resources. Although there is a remarkably pioneering study of incorporating a cloud resolving model with fine resolution (e.g., the vertical resolution is 20m and the horizontal resolution: 250m in Parishani et al. 2017) into a GCM to explicitly capture boundary layer turbulence ("ultraparameterization": Parishani et al. 2017), the computational cost is incomparably higher than conventional GCMs. Since the only option is to use GCMs for such studies, the representation of MLCs must be improved and changes in MLCs must be represented realistically in GCMs.

4.2 Various Studies Related to Future Changes in MLCs

Changes in low clouds in a warmer climate and low cloud feedback have been studied extensively in recent years, particularly with respect to tropical and subtropical low cloud. In particular, the CMIP project (CMIP5: Taylor et al. 2012, CMIP6: Eyring et al. 2016) and the Cloud Feedback Model Intercomparison Project (CFMIP2: Bony et al. 2011, CFMIP3:

Webb et al. 2017) proposed various experiments (listed in Table 2) that resulted in significant progress in understanding cloud feedback mechanisms and future changes in low clouds. Though atmosphere–ocean coupled models are used for climate projections, it is difficult to understand the mechanisms of cloud changes from such coupled simulations, because different changes in atmospheric circulation caused by differently simulated SST make the understanding of cloud changes highly complicated. Therefore, various simulations using atmospheric components, where SST is given as a boundary condition, were proposed to reveal the mechanisms. Atmospheric model simulations forced by SST observed in the past decades, known as the Atmospheric Model Intercomparison Project (AMIP), are conducted as a basic experiment. In addition, a simulation of AMIP with a globally uniform 4 K increase in SST, where CO_2 concentration is not changed, is performed to examine the effect of increased SST only; AMIP with a composite geographical pattern of SST rise obtained from CMIP3 coupled GCMs under CO_2 increase is performed to detect the effect of changes in SST patterns; and AMIP with quadrupled CO_2 is performed to isolate the cloud response to changes in CO_2 alone without changes in SST. An aqua planet experiment is performed, as well as that with a 4 K uniform increase in SST, and with quadrupled CO_2 under constant SST. This approach eliminates influences from land and topography, and can be used to isolate the effect of the oceans. To investigate the effects of aerosols, runs are performed using climatological SST with pre-industrial aerosols, with aerosols from the year 2000, and with sulfate aerosols from the year 2000 and other aerosols in the pre-industrial era. For instance, these AMIP series data with SST perturbations were used by Webb and Lock (2013) and Webb et al. (2015) for studies related to cloud feedback, and by Kawai et al. (2016, 2018) for studies of future changes in marine fog. AMIP experiments with quadrupled CO_2 were used by Kamae et al. (2015) to investigate the cloud response to increasing CO_2 without SST changes. This direct cloud response to increased greenhouse gas concentration is called ‘cloud adjustment’, in which the effect of changes in surface air temperature is mostly excluded, in contrast to cloud feedback (Kamae et al. 2015). They found that a downward shift in the low-cloud layer and a reduction in low cloud occur as a result of the adjustment. Zelinka et al. (2014) used simulation data with pre-industrial and year 2000 aerosols, and quantified components of aerosol–cloud–radiation interactions in CMIP5 multi models. For instance, they found that roughly 25% of the ensemble mean shortwave radiation change comes from radiation changes due directly to aerosol changes, and 75% comes from radiation changes through changes in clouds.

In fact, even when atmospheric simulations conducted using atmospheric components of CMIP5 climate models with a common SST field are intercompared, it is still difficult to elucidate the different mechanisms associated with cloud changes in different models in detail. This is because large-scale meteorological fields, including vertical velocity and horizontal advection, change differently in the atmospheric models, even if a common SST and SST perturbation are used for such simulations. A model intercomparison case, CGILS

[CFMIP-GCSS Intercomparison of Large-Eddy and Single-Column Models, where GCSS stands for GEWEX (Global Energy and Water Cycle Experiment) Cloud System Study], was designed by Zhang et al. (2010, 2012), based on Zhang and Bretherton (2008), to understand in detail the cloud feedback mechanism of marine low clouds in climate models. A single column model (SCM) is a vertical one-dimensional model without a dynamics scheme, which is extracted from a three-dimensional climate model, and it has the same physical schemes as the original climate model. SCMs are the most simplified versions of GCMs and used to simplify the circumstances by controlling the forcing and to understand the behavior of MLCs simulated in GCMs. Generally, horizontal advection tendencies of temperature and water vapor and the vertical velocity are given as forcings (also horizontal wind field itself or geostrophic wind is given), and temperature and water vapor profiles are calculated by the models. In the intercomparison case, three different marine low-level cloud regimes (shallow cumulus, stratocumulus, and stratus) are simulated under a control climate forcing and a future climate forcing with a 2 K increase in SST. Zhang et al. (2013) found, from the analysis of CGILS using SCMs, that SCMs in which the shallow convection scheme is active (inactive) tend to have positive (negative) cloud feedback for stratocumulus regimes (Fig. 12). They showed that shallow convection becomes more vigorous and transports more water vapor from the boundary layer to a free atmosphere in a warmer climate for models in which the shallow convection scheme is active. Brient and Bony (2013) performed several sensitivity experiments utilizing this case and discussed the relationship between changes in low-level clouds and changes in the vertical gradient of moist static energy. Blossey et al. (2013) analyzed LES results from CGILS and discussed the detailed behavior of changes in low clouds under warmer climates by decomposing roles of increased SST and weakened subsidence. Several other LES studies have investigated the responses of low clouds to global warming in other settings. Bretherton (2015) and Bretherton and Blossey (2014) discussed mechanisms related to the low cloud feedback: cloudiness reduction due to surface warming (thermodynamic effect), cloudiness reduction due to CO_2- and H_2O-induced increase in atmospheric emissivity aloft (radiative effect), cloudiness increase due to increased lower tropospheric stratification (stability effect), and cloudiness increase due to reduced subsidence (dynamic effect). They concluded that cloud decreases in warmer climates and the low cloud feedback is positive as results of the four mechanisms.

Recent studies based on observational relationships and GCMs also tend to support decreases in low cloud cover in warmer climates and the positive low cloud feedback (e.g., Klein et al. 2017, Nuijens and Siebesma 2019). It is shown that decrease in low cloud cover in warmer climates is plausible based on CMIP5 multi-model simulation data (Qu et al. 2014, 2015) and observational relationships (e.g. Kawai et al. 2017). It is also revealed that majorities of CMIP5 multi-models (Zelinka et al. 2013) and CMIP 6 multi-models (Zelinka et al. 2020) show positive low clod feedback.

5. Parameterization of MLCs

5.1 Parameterization of Clouds

A typical horizontal width of a grid box in GCMs is 100 to 200 km, and that in global NWP models is 15 to 50 km (note that the actual shape of a grid box is like a thin plate that has a horizontal size of ~100 km and ~0.2 km thick rather than a box). However, clouds can be much smaller than this and may only partly cover such model grid boxes, as shown in Fig. 13. In addition, the actual effective resolution of atmospheric models is 4−6 times larger than the model grid box (e.g., Skamarock 2004, Frehlich and Sharman 2008). Therefore, the concept of cloud fraction, which is defined as a fraction of a model grid box covered by clouds, should be used instead of assigning “completely clear” or “completely cloudy” to each model grid box. The most important purpose of cloud parameterization is to determine cloud fraction and cloud water content, which is the mass ratio of cloud water to moist air, for each model grid box. Cloud water content is the sum of liquid water content and ice water content. This part of GCMs, in which subgrid-scale variability of physical variables including water vapor is essential, is sometimes called cloud “macrophysics” in contrast to cloud microphysics that refers to micro-scale physical processes related to clouds including phase change, conversion to rain, and nucleation. For instance, in the case of relative humidity of 97%, cloud fraction of the grid box can vary from 0% to near 100% (e.g. 80%) depending on the assumed subgrid-scale variability in the grid box, accompanied by the corresponding cloud water content.

a. Calculation of cloud fraction and cloud water content

There are three ways to determine a pair of cloud fraction and cloud water content values for each model grid. The first is to calculate cloud water content prognostically and determine cloud fraction diagnostically (e.g., Sundqvist et al. 1989):

$$\frac{\partial \overline{q_c}}{\partial t} = \mathrm{adv}(\overline{q_c}) + S_{\mathrm{conv}} + S_{\mathrm{strt}} - E - G, \tag{1}$$

$$A = f(\overline{\mathrm{RH}}), \quad \text{or} \quad f(\overline{\mathrm{RH}}, \overline{q_c}) \quad \text{etc.,} \tag{2}$$

where q_c (kg kg^{-1}) is cloud water content; $\mathrm{adv}(\ )$ is an advection term; S_{conv} and S_{strt} (kg kg^{-1} s^{-1}) are production terms related to convection and stratiform, respectively; E and G (kg kg^{-1} s^{-1}) are dissipation terms due to evaporation and conversion into precipitation, respectively; A (non-dimensional) is the cloud fraction; and RH (non-dimensional) is relative humidity. To clearly distinguish grid-box-average and sub-grid-box values, overbars are used to denote the spatial average in each model grid box. In this method, cloud water content is integrated timestep-by-timestep using the equation of temporal differentiation, and the cloud fraction is calculated simply as a function of, for example, relative humidity.

The second way is to calculate both cloud water content and cloud fraction prognostically (e.g., Tiedtke 1993, Mannoji 1995):

$$\frac{\partial \overline{q_c}}{\partial t} = \mathrm{adv}(\overline{q_c}) + S_{\mathrm{conv}} + S_{\mathrm{strt}} - E - G, \tag{3}$$

$$\frac{\partial A}{\partial t} = \mathrm{adv}(A) + AS_{\mathrm{conv}} + AS_{\mathrm{strt}} - AE - AG, \tag{4}$$

where AS_{conv}, AS_{strt}, AE, and AG (s^{-1}) are similar to S_{conv}, S_{strt}, E, and G but for cloud fraction, respectively. In this method, both cloud water content and cloud fraction are integrated using the differential equations in time, respectively.

The third way to calculate cloud fraction and cloud water content is a cloud scheme in which the prognostic variables are total water content $\overline{q_t}$ (= $\overline{q} + \overline{q_c}$) (kg kg^{-1}) and liquid–frozen water temperature $\overline{T_L}$ (= $\overline{T} - L/c_p \cdot \overline{q_c}$) (K), where q (kg kg^{-1}) is specific humidity, T (K) is temperature, L (J kg^{-1}) is latent heat (the sum of latent heat of evaporation and fusion is used as for ice clouds), and c_p (J K^{-1} kg^{-1}) is the specific heat at constant pressure. The set of variables $\overline{q_t}$ and $\overline{T_L}$ is used because they are conserved during phase changes of cloud water ('cloud-conserved variables'; Smith 1990). These variables do not change even when clouds evaporate or form from water vapor, or when liquid clouds freeze or ice clouds melt in the grid box. A pair of cloud water content and cloud fraction values is then mathematically deduced from these variables using assumed probability density functions (PDFs) (e.g., Mellor 1977, Sommeria and Deardorff 1977, Smith 1990, Le Treut and Li 1991). Calculations using this method are as follows:

$$\overline{q_c} = f_1(\overline{q_t}, \overline{T_L}), \tag{5}$$

$$A = f_2(\overline{q_t}, \overline{T_L}), \tag{6}$$

where f_1 and f_2 are uniquely determined using assumed PDF shapes for q_t and T_{L}. A schematic of this PDF-based cloud scheme is shown in Fig. 14. Cloud fraction is calculated as an area of the PDF where q_t is larger than the saturation specific humidity $\overline{q_s}$ (kg kg^{-1}). Cloud water content is calculated as the integrated value of $q_t - \overline{q_s}$ weighted by the PDF of

q_t (the first moment of the PDF of q_t) for q_t larger than the saturation specific humidity, as shown in the equation in Fig. 14. Here, we ignore the subgrid-scale inhomogeneity of temperature (or liquid–frozen water temperature) for simplicity, and discuss the inhomogeneity of humidity only. In these types of scheme, the PDF of total water content is a key element and is necessary for the calculations. Furthermore, the PDFs of water vapor and cloud water are implicitly assumed as well in the first and second methods described above, where $\overline{q_c}$ is a prognostic variable. As shown in Fig. 15, for instance, the Sundqvist scheme assumes delta functions for both the clear part and the cloudy part, while the Tiedtke scheme assumes a uniform top hat function for the clear part and a delta function for the cloudy part.

Generally, in the state-of-the-art GCMs and operational global weather prediction models, their cloud macrophysics are still based on one of these three ways, although they have liquid and ice water contents as separated prognostic variables and some of the models have prognostic number concentrations of droplets and ice crystals. For instance, the Max Planck Institute for Meteorology Earth System Model version 1.2 (MPI-ESM1.2) (Mauritsen et al. 2019) utilizes Sundqvist et al. (1989) scheme as their cloud macrophysics, and it is based on the aforementioned first way. A GCM MRI-ESM2 (Yukimoto et al. 2019) and the European Centre for Medium-Range Weather Forecasts (ECMWF) operational global model Integrated Forecasting System (IFS) (ECMWF 2019) basically utilize Tiedtke (1993) scheme, and the Met Office climate model HadGEM3 (Williams et al. 2018, Walters et al.

2017) adopts Wilson et al. (2008) scheme as their cloud macrophysics, and they are based on the aforementioned second way. A GCM MIROC6 (Tatebe et al. 2019) utilizes Watanabe et al. (2009) scheme and the JMA operational global model Global Spectral Model (JMA 2019) adopts Smith (1990) scheme, and they are based on the aforementioned third way. As examples of the third way, there are advanced attempts to unify cloud macrophysics, boundary layer turbulence, and shallow convection schemes using common PDFs, such as the Cloud Layers Unified by Binormals (CLUBB) scheme (e.g., Guo et al. 2014, Guo et al. 2015, Bogenschutz et al. 2013). In a version of CLUBB, not only PDFs of total water content and liquid-frozen water temperature, but also sub-grid PDFs of vertical velocity are explicitly taken into account (Guo et al. 2014): vertical velocity PDFs are used for calculation of aerosol activation that determines cloud droplet number concentration.

b. Probability density functions

The PDFs have been given just as assumed ones in many previous studies related to cloud parameterization (e.g., a Gaussian distribution: Sommeria and Deardorff 1977, Mellor 1977; a triangular distribution: Smith 1990; a uniform distribution: Le Treut and Li 1991). Other studies have examined PDF shapes using CRMs or LES models (e.g., Laplace and exponential distributions: Bougeault 1981, Xu and Randall 1996; a gamma distribution: Bougeault 1982; a beta distribution: Tompkins 2002; binormal distributions: Lewellen and Yoh 1993; a skewed-triangular distribution: Watanabe et al. 2009). Several studies have investigated these PDFs based on observations such as aircraft data (e.g., Wood and Field 2000, Larson et al. 2002) or satellite data (e.g., Considine et al. 1997, Wood and Hartmann 2006). For instance, Kawai and Teixeira (2010, 2012) used satellite data to show that the PDFs vary depending on the cloud regimes (Fig. 16) and the shape of the PDFs is highly correlated with the stabilities of the lower troposphere.

Not only the shape of PDFs but also the width of the PDFs is important in PDF-based cloud schemes. In the original concept of PDF based cloud schemes (e.g. Sommeria and Deardorff 1977, Mellor 1977) the widths of PDFs were supposed to be obtained from turbulence schemes. However, such widths from turbulence schemes are too small for PDF-based cloud schemes used in GCMs or NWP models, because the widths are not determined by the fluctuations at the turbulence scale but mainly by meso-scale fluctuations. Therefore, it is impossible to obtain PDF information from turbulence schemes and more practical ways are adopted in GCMs and NWP models (e.g., Smith 1990). In fact, it is difficult to determine the widths simply, because the widths must vary depending on structures or morphologies of cloud regimes, altitude, and meteorological conditions as well as the shape of PDFs.

c. Calculations of precipitation and radiation from clouds

In cloud parameterizations, the dissipation terms of cloud water content such as those due to conversion into precipitation must be calculated in addition to the terms associated with cloud formation. In PDF-based cloud schemes, these dissipation terms are calculated after cloud water content is determined by Eq. (5). As an example of such terms, autoconversion is commonly used to calculate conversion of cloud water content to precipitation in large-scale models (e.g., Sundqvist 1978, Rotstayn 1997). The autoconversion rate (the conversion rate of cloud water content to precipitation), is assumed to be proportional to the αth power of cloud water content. The cloud water content and cloud fraction thus obtained are used not only in moist processes, but also radiation processes; for instance, shortwave reflectance, which is the ratio of reflected radiation to incident radiation, is calculated from vertically integrated cloud water content.

Grid-box-average values of cloud water content have been commonly used to calculate autoconversion rate. Generally, grid-box-average values of integrated cloud water content are also used for the calculation of shortwave reflectance in a radiation process. This means that horizontal homogeneity of cloud water content is assumed for those calculations, even though cloud water content is in fact horizontally inhomogeneous. However, inhomogeneously distributed cloud water content in a model grid-box gives different autoconversion rates of cloud water to precipitation in the moist processes (e.g., Larson et al. 2001, Wood et al. 2002, Kawai and Teixeira 2012) and a different albedo in the radiation processes (e.g., based on observations: Cahalan et al. 1994, Barker et al. 1996, Pincus et al. 1999, Oreopoulos and Cahalan 2005, Kawai and Teixeira 2012; based on large eddy simulations: Kogan et al. 1995, Bäuml et al. 2004, de Roode and Los 2008) from the homogeneously distributed case, even though the average cloud water content in the model grid box is the same. Thus, PDF information is needed for two steps in model calculations (Fig. 17): PDFs of humidity (and temperature) are required to determine a pair of cloud fraction and cloud water content at the first step, and PDFs of cloud water content to determine the inhomogeneity effect on, for instance, calculations of autoconversion and albedo, at the second step.

Several studies have investigated inhomogeneity effects of cloud microphysics including autoconversion rate and radiation calculation in GCMs. For instance, Morrison and Gettelman (2008) implemented an inhomogeneity effect of cloud microphysics in their GCM assuming a gamma function, and their cloud microphysics is also used in Guo et al. (2014). Hotta et al. (2020) investigated an inhomogeneity effect of autoconversion rate in their GCM using a triangular function that is also used for their cloud macrophysics. Hill et al. (2015) investigated inhomogeneity effects both of cloud microphysics and radiation calculation in their GCM using a parameter of inhomogeneity obtained from satellite observation, which depends on the cloud regimes. However, at present, these PDFs used for cloud macrophysics and inhomogeneity effects for cloud microphysics and radiation process are not treated consistently in many GCMs and global NWP models.

5.2 Difficulties in Parameterization of MLCs

Even when the cloud schemes introduced in Section 5.1 are applied, MLCs are not easily reproduced in GCMs and NWP models. The main reason for this is that interactions of the many physical processes related to MLCs are complicated, and the model layers are not thin enough in the vertical to represent processes related to MLCs (as discussed in Section 2.3). Mid- and high-level clouds can be represented by the aforementioned cloud schemes to some extent because the cloud fraction is generally related to relative humidity in such schemes and mid- and high-level clouds in nature have some correlation with grid-scale relative humidity. However, even very small tendencies in the formation and dissipation terms can form or destroy MLCs, and furthermore, relative humidity can be strongly controlled by cloud cover itself for MLCs, while updraft of air, which is determined mainly by large-scale convergence, controls relative humidity for mid- and high-level clouds.

Therefore, various specific schemes and treatments have been proposed to represent MLCs in models. For instance, Slingo (1980, 1987) and Teixeira and Hogan (2002) proposed diagnostic cloud amount schemes specialized for MLCs, which are incorporated into diagnostic cloud schemes based on relative humidity. They used inversion strength to determine stratocumulus cloud amount because stratocumulus clouds could not be reproduced by diagnostic cloud schemes based only on relative humidity. For instance, Kawai and Inoue (2006) showed that the representation of stratocumulus in GSM, which is a global operational model at the JMA, was dramatically improved by the implementation of a simple stratocumulus scheme based on Slingo (1980, 1987), although the model could not have represented any subtropical stratocumulus clouds until 2004.

To reproduce MLCs based on physics, it is particularly important to represent accurately the mixing of air at the top of clouds, including cloud top entrainment. Therefore, not only the cloud scheme, but also the turbulence scheme must be developed simultaneously or as a combination in order to represent MLCs. Figure 18 shows that subtropical stratocumulus is well represented in MRI-ESM2 (Yukimoto et al. 2019), in which turbulent mixing at the top of the cloud layer is strongly suppressed in conditions where stratocumulus is likely to form (Kawai et al. 2019). However, this figure shows that the stratocumulus disappears when this treatment (scheme) is turned off. Lock et al. (2000) proposed a boundary layer mixing scheme in which the boundary layer is classified into six types and the diffusion coefficient is calculated differently for each type; e.g., cumulus-capped, stratocumulus over cumulus, stratocumulus not over cumulus, and mixed layer with stratocumulus, with an explicit parameterization of cloud top entrainment.

Shallow convection schemes are also important because they significantly modify MLC coverage (e.g., Park and Bretherton 2009, Ogura et al. 2017); more active shallow convection results in smaller MLC coverage, as mentioned in Section 4.2. Zhao et al. (2018) showed that subtropical stratocumulus can be successfully increased by turning off shallow convection where EIS is larger than a threshold value (that is, favorable condition for stratocumulus) in Geophysical Fluid Dynamics Laboratory (GFDL) Global Atmosphere Model AM4.0. The ECMWF operational global model also uses this treatment (ECMWF 2019). Kawai et al. (2019) showed that the vertical structure of low clouds in the area of stratocumulus to cumulus transition is improved and low cloud cover is increased also in the Southern Ocean together with a reduction in the radiation bias by turning off shallow convection when ECTEI is larger than a threshold value in MRI-ESM2.

In recent years, it has been recognized that the occurrence frequency of tropical and subtropical marine low clouds is too low but the albedo of the cloudy part of such clouds is too high, although the radiative flux errors are compensated by these two errors. This is known as the ‘too few, too bright low-cloud problem’ (e.g., Zhang et al. 2005, Karlsson et al. 2008, Nam et al. 2012). Some studies suggest that an insufficient vertical resolution in GCMs can cause this problem (e.g., Konsta et al. 2016). Several methods that compensate for insufficient vertical resolution have been developed, including the use of vertical sublevels (Wilson et al. 2007). Brooks et al. (2005) proposed the introduction of areal cloud fraction, which is different from volume cloud fraction, although these two cloud fractions are identical in conventional GCMs under the assumption of vertically homogeneous cloud in each model vertical layer.

6. Other modeling issues related to MLCs in GCMs

The main purpose in the parameterization part of this paper is to introduce the basics of cloud macrophysics that directly determine cloud fraction and cloud water content in GCMs. Obviously, changes in cloud fraction and cloud water content in warmer climates are important for climate simulations. However, there are other factors related to low clouds that affect climate simulations. Figure 19 summarizes low cloud properties important for climate simulations and the physical processes that mainly determine them in GCMs. One of the major factors is a cloud phase change (ice to liquid) in warmer climates that is related to cloud microphysics in GCMs. Another is a change in radiative flux due to aerosol–cloud interaction in different aerosol climates. Therefore, we briefly mention these two issues in the context of parameterizations in GCMs and their difficulties.

6.1 Liquid and ice clouds (Cloud microphysics)

A significant lack of clouds and/or optical thickness over the Southern Ocean is a serious problem in most climate models, and it causes huge biases in shortwave radiative flux over the Southern Ocean, especially in the summer months (Trenberth and Fasullo 2010). Although the causes of this problem include a lack of cloud fraction and insufficient cloud number concentration due to a lack of cloud condensation nuclei, some studies have pointed out that the lack of supercooled liquid water in GCMs is a source of insufficient solar reflectance of clouds over the Southern Ocean (e.g., Bodas-Salcedo et al. 2016, Kay et al. 2016). At the temperature of the marine boundary layer over the Southern Ocean, liquid phase and ice phase clouds can coexist. Liquid clouds are optically thicker than ice clouds if the cloud (liquid + ice) water content is the same because the size (r_c) of cloud droplets is much smaller than that of ice crystals and this corresponds to a larger number concentration for cloud droplets. In this case, the sum of the scattering cross-sections of cloud particles that essentially determines optical thickness is increased, largely because the contribution of increased number concentration ($\propto r_c^{-3}$) is more significant than that of decreased scattering cross-sections of each particle ($\propto r_c^2$). In recent years, Cloud–Aerosol Lidar and Infrared Pathfinder Satellite Observations (CALIPSO; Winker et al. 2009) data have revealed that the ratio of liquid phase at the temperature of the mixed phase is much larger than expected (e.g., Hu et al. 2010, Cesana and Chepfer 2013). McCoy et al. (2015) compared the phase ratio in CMIP5 models and CALIPSO observations and found that the phase ratios in CMIP5 models vary widely and the ratio of liquid phase (supercooled water) in most models is much smaller than that observed.

Another issue is related to low cloud feedback especially over the Southern Ocean. If ice clouds change to liquid clouds in warmer climates due to increasing temperature, the optical thickness of clouds increases and suppresses the temperature increase due to greenhouse gases (negative cloud feedback). However, this negative feedback does not happen if the clouds are already liquid clouds in the present climate. Therefore, cloud phase is also an important factor for climate simulations and the importance of this feedback especially over the Southern Ocean has been studied by many researchers (Tsushima et al. 2006, McCoy et al. 2015, Bodas-Salcedo et al. 2016, Kay et al. 2016, Tan et al. 2016, Frey and Kay 2018).

A great amount of effort is being devoted to solve this issue of insufficient supercooled liquid clouds by modelers. For instance, Forbes et al. (2011) successfully increased the ratio of supercooled liquid water and reduced shortwave radiation bias over the Southern Ocean in the ECMWF global model, by reduction in the ice deposition rate at cloud top in the cloud microphysics. In the Community Atmosphere Model CAM6, the shortwave radiation bias over the Southern Ocean due to insufficient supercooled liquid water was ameliorated by the new ice nucleation scheme and the new prognostic microphysics scheme (Bogenschutz et al. 2018). In the Met Office climate model HadGEM3, the similar radiation bias was improved due to increase in supercooled liquid water by introducing turbulent production of liquid water in mixed-phase clouds (Williams et al. 2018, Walters et al. 2017, Furtado et al. 2016). Kawai et al. (2019) achieved the increase in the ratio of supercooled liquid water by utilizing an observed relationship for determining the liquid-ice ratio in a source term of cloud water in MRI-ESM2. Zelinka et al. (2020) showed that the ratio of supercooled liquid water is increased in CMIP6 multi-models from CMIP5 multi-models, and it could be a reason for larger temperature increase in CMIP6 multi-models than in CMIP5 multi-models.

The cloud phase is generally calculated by the cloud microphysics in models. Although cloud microphysics is beyond the scope of this paper, some of the difficulties concerning the usage of microphysics schemes in GCMs or global NWP models are briefly introduced here. One problem is that a long time step is used in these models although cloud microphysics includes many processes that have short time scales. For instance, the time step used in MRI-ESM2 (Yukimoto et al. 2019) for TL159 simulations submitted to CMIP6 is 30 minutes. However, a time step should be less than several tens of seconds for an appropriate calculation of cloud microphysics (e.g., Barrett et al. 2019, Posselt and Lohmann 2008, Michibata et al. 2019). One solution to the problem of long time steps is for short time-scale processes including cloud microphysics and turbulence to be calculated several times using sub-time-steps within one model integration time step (e.g., Posselt and Lohmann 2008, Gettelman et al. 2015, Michibata et al. 2019). However, in practice it is difficult to adopt a sub-time-step that is short enough for cloud microphysics in climate simulations or operational global simulations due to their computational cost. Forbes et al. (2011) developed an implicit approach to calculate the microphysics process stably for a long time step in the ECMWF operational global model.

Another issue is that global NWP models and GCMs have large grid boxes of 20 to 200 km and the microphysics cannot assume that a whole grid box has homogeneous grid-box-average values. Although it is obviously necessary to discriminate between cloudy and clear parts in a model grid box, this discrimination is far from sufficient. For instance, there should be mixed-phase parts, ice-only parts and liquid-only parts in the cloudy volume corresponding to the model grid box size (Tan and Storelvmo 2016). Wilson et al. (2008) developed a prognostic cloud fraction and condensation scheme, in which liquid only area, ice only area, mixed phase area, and clear area exist in one model grid box and three different cloud fractions corresponding to liquid only, ice only and mixed phase areas are prognostic variables. Although this is already a complicated scheme, it still requires many simplifying assumptions. The complexity dramatically increases if we try to simulate clouds in a more realistic way. This is a very bothersome problem and we need to develop a parameterization that is simple enough to implement in GCMs and can still reproduce real clouds adequately.

6.2 Aerosol cloud interactions

In climate simulations, in addition to changes in clouds due to temperature increase caused by increased greenhouse gas concentration, the changes in clouds due to changes in aerosol concentration are important for estimating accurate temperature increase in the future climate. Because this topic is also beyond the scope of this paper, only the basic concept and the associated uncertainty are briefly introduced below.

Cloud particles are formed from aerosol particles, where aerosol particles work as cloud condensation or ice nuclei (e.g., Rogers and Yau 1996). Therefore, aerosol particles must be intrinsically important for cloud formation. Particularly from the viewpoint of climate studies and the effect on radiative flux, the influence of aerosols on clouds is referred to as aerosol–cloud interaction or the aerosol indirect effect (Lohmann and Feichter 2005). There are two kinds of aerosol–cloud interactions; one is referred to as the cloud-albedo effect or the first indirect effect, and another as the cloud-lifetime effect or the second indirect effect. When aerosols are abundant, the number concentration of cloud particles must increase. If cloud water content does not change in the abundant aerosol case, the cloud water is distributed over many small particles and increases the optical thickness of the clouds (Twomey 1977). This is called the Twomey effect, cloud-albedo effect or the first indirect effect. If aerosols are abundant and consequently each cloud particle is small, the conversion rate of cloud particles to rain or snow must be slower and the lifetime of cloud particles and the liquid water path will increase (Albrecht 1989). This is called the cloud-lifetime effect or the second indirect effect. Note that although the term 'lifetime' is used, this effect is often defined by changes in liquid water path with respect to changes in the number concentration of aerosols or cloud droplets, because lifetime itself is not easily measured.

However, these aerosol–cloud interactions have not been implemented in operational global NWP models. For instance, the GSM of JMA does not incorporate them even now (JMA 2019), although the forecast skill of this model is relatively high. This is because relative humidity is the dominant factor determining cloud variations on hourly or daily time scales. On the other hand, aerosol–cloud interactions are critically important for climate simulations where the spatial cloud patterns evident in snapshots and temporal variations of clouds vanish with averaging. Because a change in global radiative flux of the order of no more than 1 W m^{-2} significantly influences the results in climate simulations (note that the radiative forcing of the CO_2 increase in the past 100 years is less than 2 W m^{-2} ; Myhre et al. 2013), the slight change in optical thickness of clouds due to aerosol–cloud interactions has a significant influence on such simulations. If we do not implement aerosol–cloud interactions in GCMs, the simulated surface temperature increase in the 20th century is overestimated because aerosols increased in the 20th century and the aerosol–cloud interactions should have suppressed the temperature increase to some extent. Therefore, many GCMs implement aerosol–cloud interactions. For instance, not only liquid and ice water content but also their number concentrations are prognostic variables in MRI-CGCM3 (Yukimoto et al. 2012) and MRI-ESM2 (Yukimoto et al. 2019) and aerosol–cloud interactions are incorporated in the model. In contrast, the number concentrations of cloud droplets and ice crystals are not prognostic variables and the effective radii of cloud droplets are not affected by aerosol concentrations in the JMA GSM.

On the other hand, there are still large uncertainties associated with aerosol–cloud interactions. Recently, several studies using satellite observations showed that the cloud-lifetime effect for liquid clouds is much smaller than expected and almost all GCMs overestimate the effect (e.g., Quaas et al. 2009, Wang et al. 2012), although the magnitude of the cloud-albedo effect is consistent between observations and GCMs (e.g., Quaas et al. 2009, Gryspeerdt et al. 2020). This inconsistency is currently being debated (e.g., Isaksen et al. 2009). Even the opposite effect has been proposed recently, in which a reduction in LWP (e.g., Michibata et al. 2016, Sato et al. 2018a) and a reduction in lifetime occur (e.g., Haywood et al. 2009) when aerosols increase. Furthermore, aerosol–cloud interactions for ice clouds are less well understood than those for liquid clouds because the formation process of ice crystals is much more complicated than that of cloud droplets. The aerosol–cloud interactions for liquid and ice clouds will be studied extensively by the climate and cloud communities over the next couple of decades.

7. Conclusions

One purpose of this review paper is to provide the basic knowledge of marine low clouds and explain the importance of such clouds in climate simulations for readers with a range of meteorological backgrounds who may not be as familiar with low clouds as they are with convective and precipitating clouds. Another purpose is to introduce the concept of parameterization of the clouds in GCMs and the associated difficulties.

An introduction to marine low clouds was provided in Section 2, including their global distribution, important physical processes related to the clouds such as cloud top entrainment, and basic characteristics such as diurnal variations. Some observational and modeling studies of such clouds were introduced in Section 3. Subsequently, in Section 4, the considerable importance of low cloud change for climate simulations was explained and some recent studies were introduced. The representation of MLCs in GCMs was confirmed to be the main source of uncertainties in predicted temperature increases in global warming simulations.

In the latter half of this paper, cloud parameterizations and some difficulties related to the representations of clouds in GCMs were introduced. In Section 5, a basic review of cloud macrophysics was given in terms of the schemes to determine cloud fraction and cloud water content in each model grid box under the assumption of subgrid-scale inhomogeneity of water vapor and cloud water. In Section 6, other topics including the difficulties and the uncertainties in representing cloud phase and aerosol–cloud interactions in GCMs were briefly introduced, because they exert a significant influence on climate simulations. In Sections 5 and 6, we highlighted the difficulties of the parameterizations in GCMs that need to be tackled by this community in the coming decades as well as explaining the basic concepts. Efforts to develop these parameterizations are still absolutely necessary, because the horizontal resolution of GCMs is not improving rapidly: the horizonal resolution is still about 100 km in major CMIP models, though the resolution was several hundred kilometers a few decades ago. Although some of the issues introduced in this paper are particularly difficult, the representation of clouds in GCMs, including subtropical stratocumulus and the Southern Ocean clouds, has gradually been improved in recent decades through the untiring effort and ingenuity of modelers, as briefly explained in Sections 5.2 and 6.1. We hope that these sections will be helpful for researchers who are not modelers but who analyze cloud data from climate simulations such as CMIP data. In addition, we would be delighted if this paper motivates researchers to work on tackling these difficult issues and solving some of them to contribute to reducing the uncertainties of climate simulations.

Acknowledgments

This review paper was developed from the Introduction section of HK's Ph.D. thesis, and HK thanks his Ph.D. thesis committee members at Kyoto University. We thank the chief editor Dr. Masaki Satoh for giving us the opportunity to write this review paper. We acknowledge the editor Dr. Akira Noda and the two anonymous reviewers for their supportive and insightful comments. This study was partly supported by the Integrated Research Program for Advancing Climate Models: TOUGOU from the Ministry of Education, Culture, Sports, Science and Technology (MEXT), Japan. Additionally, it was supported by the Japan Society for the Promotion of Science (JSPS) KAKENHI Grant Numbers JP18H03363, JP19K03977, and JP19H05699. The ERA-Interim data were provided by ECMWF. The ISCCP data were obtained from the NASA Langley Atmospheric Science Data Center. Some processed data were provided by Tsuyoshi Koshiro. Mrs. Megumi Eguchi helped edit this manuscript.

References

Albrecht, B. A., 1989: Aerosols, cloud microphysics, and fractional cloudiness. *Science*, **245**, 1227–1230.

Albrecht, B. A., D. A. Randall, and S. Nicholls, 1988: Observations of marine stratocumulus clouds during FIRE. *Bull. Amer. Meteor. Soc.*, **69**, 618–626.

Albrecht, B. A., C. S. Bretherton, D. Johnson, W. H. Scubert, and A. S. Frisch, 1995: The Atlantic Stratocumulus Transition Experiment - ASTEX. *Bull. Amer. Meteor. Soc*., **76**, 889–904.

Barker, H. W., B. A. Wiellicki, and L. Parker, 1996: A Parameterization for computing grid-averaged solar fluxes for inhomogeneous marine boundary layer clouds. Part II: Validation using satellite data. *J. Atmos. Sci.*, **53**, 2304–2316, https://doi.org/10.1175/1520-0469(1996)053<2304:APFCGA>2.0.CO;2.

Barrett, A. I., C. Wellmann, A. Seifert, C. Hoose, B. Vogel, and M. Kunz, 2019: One step at a time: How model time step significantly affects convection‐permitting simulations. *J. Adv. Model. Earth Syst.*, **11**, 641–658, https://doi.org/10.1029/2018MS001418.

Bäuml, G., A. Chlond, and E. Roeckner, 2004: Estimating PPH-bias for simulations of convective and stratiform clouds. *Atmos. Res.*, **72**, 317-328.

Betts, A. K., 1990: Diurnal variation of California coastal stratocumulus from two days of boundary layer soundings. *Tellus A*, **42**, 302–304.

Betts, A. K., and R. Boers, 1990: A cloudiness transition in a marine boundary layer. *J. Atmos. Sci.*, **47**, 1480–1497.

Blaskovic, M., R. Davies, and J. B. Snider, 1991: Diurnal variation of marine stratocumulus over San Nicolas Island during July 1987. *Mon. Wea. Rev*., **119**, 1469–1478.

Blossey, P. N., and Coauthors, 2013: Marine low cloud sensitivity to an idealized climate change: The CGILS LES intercomparison. *J. Adv. Model. Earth Syst.*, **5**, 234–258, doi:10.1002/jame.20025.

Bodas-Salcedo, A., P. G. Hill, K. Furtado, K. D. Williams, P. R. Field, J. C. Manners, P. Hyder, and S. Kato, 2016: Large contribution of supercooled liquid clouds to the solar radiation budget of the Southern Ocean. *J. Climate*, **29**, 4213–4228, https://doi.org/10.1175/JCLI-D-15-0564.1.

Bogenschutz, P. A., A. Gettelman, H. Morrison, V. E. Larson, C. Craig, and D. P. Schanen, 2013: Higher-order turbulence closure and its impact on climate simulations in the Community Atmosphere Model. *J. Climate*, **26**, 9655–9676, https://doi.org/10.1175/JCLI-D-13-00075.1.

Bogenschutz, P. A., A. Gettelman, C. Hannay, V. E. Larson, R. B. Neale, C. Craig, and C.-C. Chen, 2018: The path to CAM6: coupled simulations with CAM5.4 and CAM5.5. *Geosci. Model Dev.*, **11**, 235–255, https://doi.org/10.5194/gmd-11-235-2018.

Bony, S., and J.-L. Dufresne, 2005: Marine boundary layer clouds at the heart of tropical cloud feedback uncertainties in climate models. *Geophys. Res. Lett.,* **32**, L20806, doi:10.1029/2005GL023851.

Bony, S., R. Colman, V. M. Kattsov, R. P. Allan, C. S. Bretherton, J. L. Dufresne, A. Hall, S. Hallegatte, M. M. Holland, W. Ingram, D. A. Randall, B. J. Soden, G. Tselioudis, and M. J. Webb, 2006: How well do we understand and evaluate climate change feedback processes? *J. Climate*, **19**, 3445–3482.

Bony, S., M. Webb, C. Bretherton, S. Klein, P. Siebesma, G. Tselioudis, and M. Zhang, 2011: CFMIP: Towards a better evaluation and understanding of clouds and cloud feedbacks in CMIP5 models. *Clivar Exch.*, **56**, 2.

Bony, S., and Coauthors, 2017: EUREC^{4}A: A field campaign to elucidate the couplings between clouds, convection and circulation. *Surv. Geophys.*, **38**, 1529–1568, https://doi.org/10.1007/s10712-017-9428-0.

Boucher, O., D. Randall, P. Artaxo, C. Bretherton, G. Feingold, P. Forster, V.-M. Kerminen, Y. Kondo, H. Liao, U. Lohmann, P. Rasch, S. K. Satheesh, S. Sherwood, B. Stevens, and X. Y. Zhang, 2013: Clouds and Aerosols. In: Climate Change 2013: The Physical Science Basis. Contribution of Working Group I to the Fifth Assessment Report of the Intergovernmental Panel on Climate Change [Stocker, T. F., D. Qin, G.-K. Plattner, M. Tignor, S. K. Allen, J. Boschung, A. Nauels, Y. Xia, V. Bex, and P. M. Midgley (eds.)]. Cambridge University Press, Cambridge, United Kingdom and New York, NY, USA.

Bougeault, P., 1981: Modeling the trade-wind cumulus boundary layer. Part I: Testing the ensemble cloud relations against numerical data. *J. Atmos. Sci.*, **38**, 2414–2428.

Bougeault, P., 1982: Cloud-ensemble relations based on the gamma probability distribution for the higher-order models of the planetary boundary layer. *J. Atmos. Sci.*, **39**, 2691–2700.

Bretherton, C. S., 2015: Insights into low-latitude cloud feedbacks from high-resolution models. *Philos. Trans. R. Soc. A*, **373**, 20140415, https://doi.org/10.1098/rsta.2014.0415.

Bretherton, C. S., and P. N. Blossey, 2014: Low cloud reduction in a greenhouse-warmed climate: Results from Lagrangian LES of a subtropical marine cloudiness transition. *J. Adv. Model. Earth Syst.*, **6**, 91–114, doi:10.1002/2013MS000250.

Bretherton, C. S., R. Ferrari, and S. Legg, 2004a: Climate Process Teams: A new approach to improving climate models. *U.S. CLIVAR Variations*, **2**, 1, 1–6.

Bretherton, C. S., T. Uttal, C. W. Fairall, S. E. Yuter, R. A. Weller, D. Baumgardner, K. Comstock, R. Wood, and G. B. Raga, 2004b: The EPIC 2001 stratocumulus study. *Bull. Amer. Meteor. Soc.*, **85**, 967–977.

Bretherton, C. S., R. Wood, R. C. George, D. Leon, G. Allen, and X. Zheng, 2010: Southeast Pacific stratocumulus clouds, precipitation and boundary layer structure sampled along 20° S during VOCALS-REx. *Atmos. Chem. Phys.*, **10**, 10639-10654, doi:10.5194/acp-10-10639-2010.

Brient, F., and S. Bony, 2013: Interpretation of the positive low-cloud feedback predicted by a climate model under global warming. *Climate Dyn.*, **40**, 2415–2431, doi:10.1007/s00382-011-1279-7.

Brooks, M. E., R. J. Hogan, and A. J. Illingworth, 2005: Parameterizing the difference in cloud fraction defined by area and by volume as observed with Radar and Lidar. *J. Atmos. Sci.*, **62**, 2248–2260, https://doi.org/10.1175/JAS3467.1.

Burleyson, C. D., S. P. de Szoeke, S. E. Yuter, M. Wilbanks, and W. A. Brewer, 2013:

Ship-based observations of the diurnal cycle of southeast Pacific marine stratocumulus clouds and precipitation. *J. Atmos. Sci.*, **70**, 3876–3894.

Cahalan, R. F., W. Ridgway, W. J. Wiscombe, T. L. Bell, and J. B. Snider, 1994: The albedo of fractal stratocumulus clouds. *J. Atmos. Sci.*, **51**, 2434–2455.

Caldwell, P. M., Y. Zhang, and S. A. Klein, 2013: CMIP3 subtropical stratocumulus cloud feedback interpreted through a mixed-layer model. *J. Climate*, **26**, 1607–1625.

Cesana, G., and H. Chepfer, 2013: Evaluation of the cloud thermodynamic phase in a climate model using CALIPSO-GOCCP. *J. Geophys. Res. Atmos.*, **118**, 7922–7937, https://doi.org/10.1002/jgrd.50376.

Chung, D., G. Matheou, and J. Teixeira, 2012: Steady-state large-eddy simulations to study the stratocumulus to shallow cumulus cloud transition. *J. Atmos. Sci.*, **69**, 3264–3276, https://doi.org/10.1175/JAS-D-11-0256.1.

Colling, A., 2001: Ocean circulation. 2nd Edition, Open University, Butterworth-Heinemann, p286.

Considine, G., J. A. Curry, and B. Wielicki, 1997: Modeling cloud fraction and horizontal variability in marine boundary layer clouds. *J. Geophys. Res.*, **102**, 13,517–13,525.

Davidson, B., 1968: The Barbados oceanographic and meteorological experiment. *Bull. Amer. Meteor. Soc.*, **49**, 928–934.

Deardorff, J. W., 1980: Cloud top entrainment instability. *J. Atmos. Sci.*, **37**, 131–147, doi:10.1175/1520-0469(1980)037<0131:CTEI>2.0.CO;2.

Dee, D. P., and Coauthors, 2011: The ERA-Interim reanalysis: Configuration and performance of the data assimilation system. *Quart. J. Roy. Meteor. Soc.*, **137**, 553–597, doi:10.1002/qj.828.

de Roode, S. R., and A. Los, 2008: The effect of temperature and humidity fluctuations on the liquid water path of non-precipitating closed-cell stratocumulus clouds. *Quart. J. Roy. Meteor. Soc.*, **134**, 403-416.

de Roode, S. R., and P. G. Duynkerke, 1997: Observed Lagrangian transition of stratocumulus into cumulus during ASTEX: Mean state and turbulence structure. *J. Atmos. Sci.*, **54**, 2157–2173.

de Roode, S. R., and Coauthors, 2016: Large-eddy simulations of EUCLIPSE–GASS Lagrangian stratocumulus-to-cumulus transitions: mean state, turbulence, and decoupling. *J. Atmos. Sci.*, **73**, 2485–2508, doi:10.1175/JAS-D-15-0215.1.

de Szoeke, S. P., S. Yuter, D. Mechem, C. W. Fairall, C. D. Burleyson, and P. Zuidema, 2012: Observations of stratocumulus clouds and their effect on the eastern Pacific surface heat budget along 20°S. *J. Climate*, **25**, 8542–8567.

Duynkerke, P. G., and J. Teixeira, 2001: A comparison of the ECMWF reanalysis with FIRE I observations: Diurnal variation of marine stratocumulus. *J. Climate*, **14**, 1466–1478.

Eastman, R., S. G. Warren, and C. J. Hahn, 2011: Variations in cloud cover and cloud types over the ocean from surface observations, 1954-2008. *J. Climate*, **24**, 5914-5934.

ECMWF, 2019: Clouds and large-scale precipitation. IFS Documentation, European Centre for Medium-Range Weather Forecasts, CY46r1, Part IV, Chapter 7.

Eguchi, N., T. Hayasaka, and M. Sawada, 2014: Maritime-continental contrasts in the properties of low-level clouds: A case study of the summer of the 2003 Yamase, Japan, Cloud Event. *Adv. Meteorol.*, **2014**, doi:10.1155/2014/548091.

Eyring, V., S. Bony, G. A. Meehl, C. A. Senior, B. Stevens, R. J. Stouffer, and K. E. Taylor, 2016: Overview of the Coupled Model Intercomparison Project Phase 6 (CMIP6) experimental design and organization. *Geosci. Model Dev.*, **9**, 1937–1958, https://doi.org/10.5194/gmd-9-1937-2016.

Flato, G., J. Marotzke, B. Abiodun, P. Braconnot, S. C. Chou, W. Collins, P. Cox, F. Driouech, S. Emori, V. Eyring, C. Forest, P. Gleckler, E. Guilyardi, C. Jakob, V. Kattsov, C. Reason, and M. Rummukainen, 2013: Evaluation of Climate Models. In: Climate Change 2013: The Physical Science Basis. Contribution of Working Group I to the Fifth Assessment Report of the Intergovernmental Panel on Climate Change [Stocker, T. F., D. Qin, G.-K. Plattner, M. Tignor, S. K. Allen, J. Boschung, A. Nauels, Y. Xia, V. Bex, and P. M. Midgley (eds.)]. Cambridge University Press, Cambridge, United Kingdom and New York, NY, USA.

Forbes, R. M., A. M. Tompkins, and A. Untch, 2011: A new prognostic bulk microphysics scheme for the IFS. ECMWF Technical Memorandum, **649**, 28pp.

Frehlich, R., and R. Sharman, 2008: The use of structure functions and spectra from numerical model output to determine effective model resolution. *Mon. Wea. Rev.*, **136**, 1537–1553, doi:10.1175/2007mwr2250.1.

Frey, W. R., and J. E. Kay, 2018: The influence of extratropical cloud phase and amount feedbacks on climate sensitivity. *Climate Dyn.*, **50**, 3097–3116, https://doi.org/10.1007/s00382-017-3796-5.

Furtado, K., P. R. Field, I. A. Boutle, C. J. Morcrette, and J. M. Wilkinson, 2016: A physically based subgrid parameterization for the production and maintenance of mixed-phase clouds in a general circulation model. *J. Atmos. Sci.*, **73**, 279–291, https://doi.org/10.1175/JAS-D-15-0021.1.

Garay, M. J., S. P. de Szoeke, and C. M. Moroney, 2008: Comparison of marine stratocumulus cloud top heights in the southeastern Pacific retrieved from satellites with coincident ship-based observations. *J. Geophys. Res.*, **113**, D18204, doi:10.1029/2008JD009975.

Gettelman, A., H. Morrison, S. Santos, P. Bogenschutz, and P. M. Caldwell, 2015: Advanced two-moment bulk microphysics for global models. Part II: Global model solutions and aerosol–cloud interactions. *J. Climate*, **28**, 1288–1307, https://doi.org/10.1175/JCLI-D-14-00103.1.

Gryspeerdt, E., and Coauthors, 2020: Surprising similarities in model and observational aerosol radiative forcing estimates. *Atmos. Chem. Phys.*, **20**, 613–623, https://doi.org/10.5194/acp-20-613-2020.

Guo, H., J.-C. Golaz, L. J. Donner, P. Ginoux, and R. S. Hemler, 2014: Multivariate probability density functions with dynamics in the GFDL atmospheric general circulation model: Global tests. *J. Climate*, **27**, 2087–2108, https://doi.org/10.1175/JCLI-D-13-00347.1.

Guo, H., J.-C. Golaz, L. J. Donner, B. Wyman, M. Zhao, and P. Ginoux, 2015: CLUBB as a unified cloud parameterization: Opportunities and challenges. *Geophys. Res. Lett.*, **42**, 4540–4547, https://doi.org/10.1002/2015GL063672.

Hahn, C. J., and S. G. Warren, 2009: Extended edited synoptic cloud reports from ships and land stations over the globe, 1952-1996 (2009 update). NDP-026C, Carbon Dioxide Information Analysis Center, Oak Ridge National Laboratory, Oak Ridge, TN, 79 pp.

Haywood, J., L. J. Donner, A. Jones, and J.-C. Golaz, 2009: Global indirect radiative forcing caused by aerosols: IPCC (2007) and beyond. *Clouds in the Perturbed Climate System,* J. Heintzenberg and R. J. Charlson, Eds., MIT Press, 451–467.

Hill, P. G., C. J. Morcrette, and I. A. Boutle, 2015: A regime-dependent parametrization of subgrid-scale cloud water content variability. *Quart. J. Roy. Meteor. Soc.*, **141**, 1975–1986, https://doi.org/10.1002/qj.2506.

Hotta, H., K. Suzuki, D. Goto, and M. Lebsock, 2020: Climate impact of cloud water inhomogeneity through microphysical processes in a global climate model. *J. Climate*, **33**, 5195–5212, https://doi.org/10.1175/JCLI-D-19-0772.1.

Houze, R. A., 1982: Cloud clusters and large-scale vertical motions in the Tropics. *J. Meteor. Soc. Japan*, **60**, 396–410, https://doi.org/10.2151/jmsj1965.60.1_396.

Houze, R. A., 2004: Mesoscale convective systems. *Rev. Geophys.*, **42**, RG4003, https://doi.org/10.1029/2004RG000150.

Hu, Y., S. Rodier, K. M. Xu, W. Sun, J. Huang, B. Lin, P. Zhai, and D. Josset, 2010: Occurrence, liquid water content, and fraction of supercooled water clouds from combined CALIOP/IIR/MODIS measurements. *J. Geophys. Res. Atmos.*, **115**, 1–13, https://doi.org/10.1029/2009JD012384.

Isaksen, I. S. A., and Coauthors, 2009: Atmospheric composition change: Climate–Chemistry interactions. *Atmos. Environ.*, **43**, 5138–5192.

JMA, 2019: Outline of the operational numerical weather prediction at the Japan Meteorological Agency (Appendix to WMO Technical Progress Report on the Global Data-processing and Forecasting System and Numerical Weather Prediction Research). Japan Meteorological Agency. (available online at http://www.jma.go.jp/jma/jma-eng/jma-center/nwp/outline2019-nwp/index.htm)

Kamae, Y., M. Watanabe, T. Ogura, M. Yoshimori, and H. Shiogama, 2015: Rapid adjustments of cloud and hydrological cycle to increasing CO2: A review. *Current Climate Change Reports*, 103–113, doi:10.1007/s40641-015-0007-5.

Karlsson, J., G. Svensson, and H. Rodhe, 2008: Cloud radiative forcing of subtropical low level clouds in global models. *Climate Dyn.*, **30**, 779–788, https://doi.org/10.1007/s00382-007-0322-1.

Kawai, H., and T. Inoue, 2006: A simple parameterization scheme for subtropical marine stratocumulus. *SOLA*, **2**, 17-20.

Kawai, H., and J. Teixeira, 2010: Probability density functions of liquid water path and cloud amount of marine boundary layer clouds: Geographical and seasonal variations and controlling meteorological factors. *J. Climate*, **23**, 2079–2092.

Kawai, H., and J. Teixeira, 2012: Probability density functions of liquid water path and total water content of marine boundary layer clouds: Implications for cloud parameterization. *J. Climate*, **25**, 2162-2177.

Kawai, H., T. Koshiro, H. Endo, O. Arakawa, and Y. Hagihara, 2016: Changes in marine fog in a warmer climate. *Atmos. Sci. Let.*, **17**, 548-555.

Kawai, H., T. Koshiro, and M. J. Webb, 2017: Interpretation of factors controlling low cloud cover and low cloud feedback using a unified predictive index. *J. Climate*, **30**, 9119-9131.

Kawai, H., T. Koshiro, H. Endo, and O. Arakawa, 2018: Changes in marine fog over the North Pacific under different climates in CMIP5 multimodel simulations. *J. Geophys. Res. Atmos.*, **123**, 10,911-10,924.

Kawai, H., S. Yukimoto, T. Koshiro, N. Oshima, T. Tanaka, H. Yoshimura, and R. Nagasawa, 2019: Significant improvement of cloud representation in the global climate model MRI-ESM2. *Geosci. Model Dev.*, **12**, 2875–2897, https://doi.org/10.5194/gmd-12-2875-2019.

Kay, J. E., C. Wall, V. Yettella, B. Medeiros, C. Hannay, P. Caldwell, and C. Bitz, 2016: Global climate impacts of fixing the Southern Ocean shortwave radiation bias in the

Community Earth System Model (CESM). *J. Climate*, **29**, 4617–4636, https://doi.org/10.1175/JCLI-D-15-0358.1.

Klein, S. A., and D. L. Hartmann, 1993: The seasonal cycle of low stratiform clouds. *J. Climate*, **6**, 1587–1606.

Klein, S. A., A. Hall, J. R. Norris, and R. Pincus, 2017: Low-cloud feedbacks from cloud-controlling factors: A review. *Surv. Geophys.*, **38**, 1307–1329, https://doi.org/10.1007/s10712-017-9433-3.

Kodama, Y., 1997: Airmass transformation of the Yamase air-flow in the summer of 1993. *J. Meteor. Soc. Japan*, **75**, 737–751, doi:10.2151/jmsj.87.665.

Kodama, Y.-M., Y. Tomiya, and S. Asano, 2009: Air mass transformation along trajectories of airflow and its relation to vertical structures of the maritime atmosphere and clouds in Yamase events. *J. Meteor. Soc. Japan*, **87**, 665–685, doi:10.2151/jmsj.87.665.

Kogan, Z. N., D. K. Lilly, Y. L. Kogan, and V. Filyushkin, 1995: Evaluation of radiative parameterizations using an explicit cloud microphysical model. *Atmos. Res.,* **35**, 157–172.

Konsta, D., J. L. Dufresne, H. Chepfer, A. Idelkadi, and G. Cesana, 2016: Use of A-train satellite observations (CALIPSO–PARASOL) to evaluate tropical cloud properties in the LMDZ5 GCM. *Climate Dyn.*, **47**, 1263–1284, https://doi.org/10.1007/s00382-015-2900-y.

Koseki, S., T. Nakamura, H. Mitsudera, and Y. Wang, 2012: Modeling low-level clouds over the Okhotsk Sea in summer: Cloud formation and its effects on the Okhotsk high. *J.*

Geophys. Res. Atmos., **117**, D05208, https://doi.org/10.1029/2011JD016462.

Koshiro, T., M. Shiotani, H. Kawai, and S. Yukimoto, 2018: Evaluation of relationships between subtropical marine low stratiform cloudiness and estimated inversion strength in CMIP5 models using the satellite simulator package COSP. *SOLA*, **14**, 25–32.

Kuo, H.-C., and W. H. Schubert, 1988: Stability of cloud-topped boundary layers. *Quart. J. Roy. Meteor. Soc.*, **114**, 887–916, doi:10.1002/qj.49711448204.

Larson, V. E., J. C. Golaz, and W. R. Cotton, 2002: Small-scale and mesoscale variability in cloudy boundary layers: Joint probability density functions. *J. Atmos. Sci.*, **59**, 3519–3539.

Larson, V. E., R. Wood, P. R. Field, J.-C. Golaz, T. H. Vonder Haar, and W. R. Cotton, 2001: Systematic biases in the microphysics and thermodynamics of numerical models that ignore subgrid-scale variability. *J. Atmos. Sci.*, **58**, 1117–1128, https://doi.org/10.1175/1520-0469(2001)058<1117:SBITMA>2.0.CO;2.

Lauer, A., and K. Hamilton, 2013: Simulating clouds with global climate models: A comparison of CMIP5 results with CMIP3 and satellite data. *J. Climate*, **26**, 3823–3845, https://doi.org/10.1175/JCLI-D-12-00451.1.

Le Treut, H., and Z. X. Li, 1991: Sensitivity of an atmospheric general circulation model to prescribed SST changes: Feedback effects associated with the simulation of cloud optical properties. *Climate Dyn.,* **5**, 175–187.

Lewellen, W. S., and S. Yoh, 1993: Binormal model of ensemble partial cloudiness. *J.*

Atmos. Sci., **50**, 1228–1237.

Lock, A. P., 2009: Factors influencing cloud area at the capping inversion for shallow cumulus clouds. *Quart. J. Roy. Meteor. Soc.*, **135**, 941–952.

Lock, A. P., A. R. Brown, M. R. Bush, G. M. Martin, and R. N. B. Smith, 2000: A new boundary layer mixing scheme. Part I: Scheme description and single-column model tests. *Mon. Wea. Rev.*, **128**, 3187–3199.

Lohmann, U., and J. Feichter, 2005: Global indirect aerosol effects: a review. *Atmos. Chem. Phys.*, **5**, 715–737, doi:10.5194/acp-5-715-2005.

Ma, C.-C., C. R. Mechoso, A. W. Robertson, and A. Arakawa, 1996: Peruvian stratus clouds and the Tropical Pacific circulation: A coupled ocean-atmosphere GCM study. *J. Climate*, **9**, 1635–1645, https://doi.org/10.1175/1520-0442(1996)009<1635:PSCATT>2.0.CO;2.

MacVean, M. K., 1993: A numerical investigation of the criterion for cloud-top entrainment instability. *J. Atmos. Sci.*, ***50***, 2481–2495, doi:10.1175/1520-0469(1993)050<2481:ANIOTC>2.0.CO;2.

MacVean, M. K., and P. J. Mason, 1990: Cloud-top entrainment instability through small-scale mixing and its parameterization in numerical models. *J. Atmos. Sci.*, **47**, 1012–1030, doi:10.1175/1520-0469(1990)047<1012:CTEITS>2.0.CO;2.

Mannoji, N., 1995: An explicit cloud predicting scheme implemented in the Florida State University Global Spectral Model and its impact. *J. Meteor. Soc. Japan*, **73**, 993–1009.

Matheou, G., and J. Teixeira, 2019: Sensitivity to physical and numerical aspects of large-eddy simulation of stratocumulus. *Mon. Wea. Rev.*, **147**, 2621–2639, https://doi.org/10.1175/MWR-D-18-0294.1.

Mauritsen, T., and Coauthors, 2019: Developments in the MPI‐M Earth System Model version 1.2 (MPI‐ESM1.2) and its response to increasing CO_2. *J. Adv. Model. Earth Syst.*, **11**, 998–1038, https://doi.org/10.1029/2018MS001400.

McCoy, D. T., D. L. Hartmann, M. D. Zelinka, P. Ceppi, and D. P. Grosvenor, 2015: Mixed-phase cloud physics and Southern Ocean cloud feedback in climate models. *J. Geophys. Res. Atmos.*, **120**, 9539–9554, https://doi.org/10.1002/2015JD023603.

Meehl, G. A., G. J. Boer, C. Covey, M. Latif, and R. J. Stouffer, 2000: The Coupled Model Intercomparison Project (CMIP). *Bull. Amer. Meteor. Soc.*, **81**, 313–318.

Mellor, G. L., 1977: The Gaussian cloud model relations. *J. Atmos. Sci.*, **34**, 356–358.

Michibata, T., K. Suzuki, Y. Sato, and T. Takemura, 2016: The source of discrepancies in aerosol-cloud-precipitation interactions between GCM and A-Train retrievals. *Atmos. Chem. Phys.*, **16**, 15413–15424, https://doi.org/10.5194/acp-16-15413-2016.

Michibata, T., K. Suzuki, M. Sekiguchi, and T. Takemura, 2019: Prognostic precipitation in the MIROC6‐SPRINTARS GCM: Description and evaluation against satellite observations. *J. Adv. Model. Earth Syst.*, **11**, 839–860, https://doi.org/10.1029/2018MS001596.

Morrison, H., and A. Gettelman, 2008: A new two-moment bulk stratiform cloud microphysics scheme in the Community Atmosphere Model, version 3 (CAM3). Part I:

Description and numerical tests. *J. Climate*, **21**, 3642–3659, https://doi.org/10.1175/2008JCLI2105.1.

Myers, T. A., and J. R. Norris, 2013: Observational evidence that enhanced subsidence reduces subtropical marine boundary layer cloudiness. *J. Climate*, **26**, 7507–7524, https://doi.org/10.1175/JCLI-D-12-00736.1.

Myers, T. A., and J. R. Norris, 2015: On the relationships between subtropical clouds and meteorology in observations and CMIP3 and CMIP5 models. *J. Climate*, **28**, 2945–2967, https://doi.org/10.1175/JCLI-D-14-00475.1.

Myers, T. A., and J. R. Norris, 2016: Reducing the uncertainty in subtropical cloud feedback. *Geophys. Res. Lett.*, **43**, 2144–2148, https://doi.org/10.1002/2015GL067416.

Myhre, G., D. Shindell, F.-M. Bréon, W. Collins, J. Fuglestvedt, J. Huang, D. Koch, J.-F. Lamarque, D. Lee, B. Mendoza, T. Nakajima, A. Robock, G. Stephens, T. Takemura, and H. Zhang, 2013: Anthropogenic and Natural Radiative Forcing. In: Climate Change 2013: The Physical Science Basis. Contribution of Working Group I to the Fifth Assessment Report of the Intergovernmental Panel on Climate Change [Stocker, T. F., D. Qin, G.-K. Plattner, M. Tignor, S. K. Allen, J. Boschung, A. Nauels, Y. Xia, V. Bex, and P. M. Midgley (eds.)]. Cambridge University Press, Cambridge, United Kingdom and New York, NY, USA.

Nam, C., S. Bony, J. L. Dufresne, and H. Chepfer, 2012: The too few, too bright tropical low-cloud problem in CMIP5 models. *Geophys. Res. Lett.*, **39**, 1–7.

Noda, A., and K. Nakamura, 2008: Atmospheric boundary layer clouds and LES. *Kisyo Kenkyu Note*, **219**, 89–116 (in Japanese).

Noda, A. T., K. Nakamura, T. Iwasaki, and M. Satoh, 2013: A numerical study of a stratocumulus-topped boundary-layer: Relations of decaying clouds with a stability parameter across inversion. *J. Meteor. Soc. Japan*, **91**, 727–746, https://doi.org/10.2151/jmsj.2013-601.

Noda, A. T., K. Nakamura, T. Iwasaki, and M. Satoh, 2014: Responses of subtropical marine stratocumulus cloud to perturbed lower atmospheres. *SOLA*, **10**, 34–38, https://doi.org/10.2151/sola.2014-008.

Norris, J. R., 1998a: Low cloud type over the ocean from surface observations. Part I: Relationship to surface meteorology and the vertical distribution of temperature and moisture. *J. Climate*, **11**, 369–382.

Norris, J. R., 1998b: Low cloud type over the ocean from surface observations. Part II: Geographical and seasonal variations. *J. Climate*, **11**, 383–403.

Norris, J. R., and S. A. Klein, 2000: Low cloud type over the ocean from surface observations. Part III: Relationship to vertical motion and the regional surface synoptic environment. *J. Climate*, **13**, 245–256.

Nuijens, L., and A. P. Siebesma, 2019: Boundary layer clouds and convection over subtropical oceans in our current and in a warmer climate. *Curr. Clim. Chang. Reports*, **5**, 80–94, https://doi.org/10.1007/s40641-019-00126-x.

Ogura, T., and Coauthors, 2017: Effectiveness and limitations of parameter tuning in reducing biases of top-of-atmosphere radiation and clouds in MIROC version 5. *Geosci. Model Dev.*, **10**, 4647–4664, https://doi.org/10.5194/gmd-10-4647-2017.

Oreopoulos, L., and R. F. Cahalan, 2005: Cloud inhomogeneity from MODIS. *J. Climate*, **18**, 5110–5124.

Parishani, H., M. S. Pritchard, C. S. Bretherton, M. C. Wyant, and M. Khairoutdinov, 2017: Toward low-cloud-permitting cloud superparameterization with explicit boundary layer turbulence. *J. Adv. Model. Earth Syst.*, **9**, 1542–1571, https://doi.org/10.1002/2017MS000968.

Park, S., and C. S. Bretherton, 2009: The University of Washington shallow convection and moist turbulence schemes and their impact on climate simulations with the Community Atmosphere Model. *J. Climate*, **22**, 3449–3469, https://doi.org/10.1175/2008JCLI2557.1.

Pincus, R., S. A. McFarlane, and S. A. Klein, 1999: Albedo bias and the horizontal variability of clouds in subtropical marine boundary layers: Observations from ships and satellites. *J. Geophys. Res.*, **104**, 6183–6191.

Posselt, R., and U. Lohmann, 2008: Introduction of prognostic rain in ECHAM5: design and single column model simulations. *Atmos. Chem. Phys.*, **8**, 2949–2963, https://doi.org/10.5194/acp-8-2949-2008.

Qu, X., A. Hall, S. A. Klein, and P. M. Caldwell, 2014: On the spread of changes in marine low cloud cover in climate model simulations of the 21st century. *Climate Dyn.*, **42**, 2603–

2626, https://doi.org/10.1007/s00382-013-1945-z.

Qu, X., A. Hall, S. A. Klein, and A. M. Deangelis, 2015: Positive tropical marine low-cloud cover feedback inferred from cloud-controlling factors. *Geophys. Res. Lett.*, **42**, 7767–7775, https://doi.org/10.1002/2015GL065627.

Quaas, J., and Coauthors, 2009: Aerosol indirect effects – general circulation model intercomparison and evaluation with satellite data. *Atmos. Chem. Phys.*, **9**, 8697–8717, doi:10.5194/acp-9-8697-2009.

Randall, D. A., 1980: Conditional instability of the first kind upside-down. *J. Atmos. Sci.*, **37**, 125–130.

Rauber, R. M., and Coauthors, 2007: Rain in shallow cumulus over the ocean: The RICO campaign. *Bull. Amer. Meteor. Soc.*, **88**, 1912–1928, doi:10.1175/BAMS-88-12-1912.

Rogers, R. R., and M. K. Yau, 1996: A Short Course in Cloud Physics. Butterworth-Heinemann, pp 304.

Rossow, W. B., and R. A. Schiffer, 1999: Advances in understanding clouds from ISCCP. *Bull. Amer. Meteor. Soc*., **80**, 2261–2287.

Rotstayn, L. D., 1997: A physically based scheme for the treatment of stratiform clouds and precipitation in large-scale models. I: Description and evaluation of the microphysical processes. *Quart. J. Roy. Meteor. Soc*., **123**, 1227-1282.

Rozendaal, M. A., C. B. Leovy, and S. A. Klein, 1995: An observational study of diurnal variations of marine stratiform cloud. *J. Climate*, **8**, 1795–1809.

Sandu, I., and B. Stevens, 2011: On the factors modulating the stratocumulus to cumulus transitions. *J. Atmos. Sci.*, **68**, 1865–1881, https://doi.org/10.1175/2011JAS3614.1.

Sato, Y., S. Nishizawa, H. Yashiro, Y. Miyamoto, Y. Kajikawa, and H. Tomita, 2015: Impacts of cloud microphysics on trade wind cumulus: which cloud microphysics processes contribute to the diversity in a large eddy simulation? *Prog. Earth Planet. Sci.*, **2**, https://doi.org/10.1186/s40645-015-0053-6.

Sato, Y., D. Goto, T. Michibata, K. Suzuki, T. Takemura, H. Tomita, and T. Nakajima, 2018a: Aerosol effects on cloud water amounts were successfully simulated by a global cloud-system resolving model. *Nat. Commun.*, **9**, 1–7, https://doi.org/10.1038/s41467-018-03379-6.

Sato, Y., S. Shima, and H. Tomita, 2018b: Numerical convergence of shallow convection cloud field simulations: Comparison between double-moment Eulerian and particle-based Lagrangian microphysics coupled to the same dynamical core. *J. Adv. Model. Earth Syst.*, **10**, 1495–1512, https://doi.org/10.1029/2018MS001285.

Seethala, C., J. R. Norris, and T. A. Myers, 2015: How has subtropical stratocumulus and associated meteorology changed since the 1980s? *J. Climate*, **28**, 8396–8410, https://doi.org/10.1175/JCLI-D-15-0120.1.

Shige, S., Y. N. Takayabu, W.-K. Tao, and D. E. Johnson, 2004: Spectral retrieval of latent heating profiles from TRMM PR data. Part I: Development of a model-based algorithm. *J. Appl. Meteor.*, **43**, 1095–1113, https://doi.org/10.1175/1520-0450(2004)043<1095:SROLHP>2.0.CO;2.

Shimada, T., and T. Iwasaki, 2015: Two regimes of cloud water over the Okhotsk Sea and the adjacent regions around Japan in summer. *J. Geophys. Res. Atmos.*, **120**, 2407–2418, doi:10.1002/2014JD022536.

Shimada, T., M. Sawada, and T. Iwasaki, 2014: Indices of cool summer climate in northern Japan: Yamase indices. *J. Meteor. Soc. Japan*, **92**, 17–35, doi:10.2151/jmsj.2014-102.

Siebesma, A. P., C. Jakob, G. Lenderink, R. Neggers, J. Teixera, J. Calvo, A. Chlond, H. Grenier, C. Jones, M. Kohler, H. Kitagawa, P. Marquet, A. P. Lock, F. Muller, D. Olmeda, and C. Serverijns, 2004: Cloud representation in general-circulation models over the northern Pacific Ocean: A EUROCS intercomparison study. *Quart. J. Roy. Meteor. Soc.*, **130**, 3245–3267.

Skamarock, W. C., 2004: Evaluating mesoscale NWP models using kinetic energy spectra. *Mon. Wea. Rev.*, **132**, 3019–3032, doi:10.1175/MWR2830.1.

Slingo, J. M., 1980: A cloud parameterization scheme derived from GATE data for use with a numerical model. *Quart. J. Roy. Meteor. Soc.*, **106**, 747–770.

Slingo, J. M., 1987: The development and verification of a cloud prediction scheme in the ECMWF model. *Quart. J. Roy. Meteor. Soc.*, **113**, 899–927.

Smith, R. N. B., 1990: A scheme for predicting layer clouds and their water content in a general circulation model. *Quart. J. Roy. Meteor. Soc.*, **116**, 435-460.

Soden, B. J., and I. M. Held, 2006: An assessment of climate feedbacks in coupled ocean–

atmosphere models. *J. Climate*, **19**, 3354–3360.

Soden, B. J., I. M. Held, R. Colman, K. M. Shell, J. T. Kiehl, and C. A. Shields, 2008: Quantifying climate feedbacks using radiative kernels. *J. Climate*, **21**, 3504–3520.

Sommeria, G., and J. W. Deardorff, 1977: Subgrid-scale condensation in models of non-precipitating clouds. *J. Atmos. Sci.*, **34**, 345–355.

Stephens, G. L., 2005: Cloud feedbacks in the climate system: A critical review. *J. Climate*, **18**, 237–273.

Stevens, B., and Coauthors, 2003: Dynamics and chemistry of marine stratocumulus - DYCOMS-II. *Bull. Amer. Meteor. Soc.*, **84**, 579–593, doi:10.1175/BAMS-84-5-579.

Sui, C. H., M. Satoh, and K. Suzuki, 2020: Precipitation efficiency and its role in cloud-radiative feedbacks to climate variability. *J. Meteor. Soc. Japan*, **98**, 261–282, https://doi.org/10.2151/jmsj.2020-024.

Stull, R. B., 1988: An Introduction to Boundary Layer Meteorology. Kluwer Academic, 670 pp.

Su, H., and Coauthors, 2013: Diagnosis of regime-dependent cloud simulation errors in CMIP5 models using “a-Train” satellite observations and reanalysis data. *J. Geophys. Res. Atmos.*, **118**, 2762–2780.

Sundqvist, H., 1978: A parameterization scheme for non-convective condensation including prediction of cloud water content. *Quart. J. Roy. Meteor. Soc.,* **104**, 677–690.

Sundqvist, H., E. Berge, and J. E. Kristjánsson, 1989: Condensation and cloud parameterization studies with a mesoscale numerical weather prediction model. *Mon. Wea. Rev.*, **117**, 1641–1657.

Tan, I., and T. Storelvmo, 2016: Sensitivity study on the influence of cloud microphysical parameters on mixed-phase cloud thermodynamic phase partitioning in CAM5. *J. Atmos. Sci.*, **73**, 709–728, https://doi.org/10.1175/JAS-D-15-0152.1.

Tan, I., T. Storelvmo, and M. D. Zelinka, 2016: Observational constraints on mixed-phase clouds imply higher climate sensitivity. *Science*, **352**, 224–227, https://doi.org/10.1126/science.aad5300.

Tatebe, H., and Coauthors, 2019: Description and basic evaluation of simulated mean state, internal variability, and climate sensitivity in MIROC6. *Geosci. Model Dev.*, **12**, 2727–2765, https://doi.org/10.5194/gmd-12-2727-2019.

Taylor, K. E., R. J. Stouffer, and G. A. Meehl, 2012: An overview of CMIP5 and the experiment design. *Bull. Amer. Meteor. Soc.*, **93**, 485–498.

Teixeira, J., and T. F. Hogan, 2002: Boundary layer clouds in a global atmospheric model: Simple cloud cover parameterizations. *J. Climate*, **15**, 1261–1276.

Tiedtke, M., 1993: Representation of clouds in large-scale models. *Mon. Wea. Rev.*, **121**, 3040–3061.

Tompkins, A. M., 2002: A prognostic parameterization for the subgrid-scale variability of water vapor and clouds in large-scale models and its use to diagnose cloud cover. *J. Atmos. Sci.*, **59**, 1917–1942.

Trenberth, K. E., and J. T. Fasullo, 2010: Simulation of present-day and twenty-first-century energy budgets of the southern oceans. *J. Climate*, **23**, 440–454, https://doi.org/10.1175/2009JCLI3152.1.

Tsushima, Y., and Coauthors, 2006: Importance of the mixed-phase cloud distribution in the control climate for assessing the response of clouds to carbon dioxide increase: a multi-model study. *Climate Dyn.*, **27**, 113–126, https://doi.org/10.1007/s00382-006-0127-7.

Twomey, S., 1977: The influence of pollution on the shortwave albedo of clouds. *J. Atmos. Sci.*, **34**, 1149–1152.

Uppala, S. M., and Coauthors, 2005: The ERA-40 re-analysis. *Quart. J. Roy. Meteor. Soc.*, **131**, 2961–3012.

Walters, D., and Coauthors, 2017: The Met Office Unified Model Global Atmosphere 7.0/7.1 and JULES Global Land 7.0 configurations. *Geosci. Model Dev. Discuss.*, 1–78, https://doi.org/10.5194/gmd-2017-291.

Wang, M., and Coauthors, 2012: Constraining cloud lifetime effects of aerosols using A-Train satellite observations. *Geophys. Res. Lett.*, **39**, 3–9, doi:10.1029/2012GL052204.

Warren, S. G., C. J. Hahn, J. London, R. M. Chervin, and R. L. Jenne, 1988: Global distribution of total cloud cover and cloud type amounts over the ocean. NCAR/TN-317+STR, National Center for Atmospheric Research, Boulder, USA, 42 pp.

Watanabe, M., S. Emori, M. Satoh, and H. Miura, 2009: A PDF-based hybrid prognostic cloud scheme for general circulation models. *Climate Dyn.*, **33**, 795–816, https://doi.org/10.1007/s00382-008-0489-0.

Webb, M. J., and A. P. Lock, 2013: Coupling between subtropical cloud feedback and the local hydrological cycle in a climate model. *Climate Dyn.*, **41**, 1923–1939, doi:10.1007/s00382-012-1608-5.

Webb, M. J., A. P. Lock, A. Bodas-Salcedo, S. Bony, J. N. S. Cole, T. Koshiro, H. Kawai, C. Lacagnina, F. M. Selten, R. Roehrig, and B. Stevens, 2015: The diurnal cycle of marine cloud feedback in climate models. *Climate Dyn.*, **44**, 1419-1436, doi:10.1007/s00382-014-2234-1.

Webb, M. J., and Coauthors, 2017: The Cloud Feedback Model Intercomparison Project (CFMIP) contribution to CMIP6. *Geosci. Model Dev.,* **10**, 359–384, https://doi.org/10.5194/gmd-10-359-2017.

Williams, K. D., and Coauthors, 2018: The Met Office Global Coupled Model 3.0 and 3.1 (GC3.0 and GC3.1) configurations. *J. Adv. Model. Earth Syst.*, **10**, 357–380, https://doi.org/10.1002/2017MS001115.

Wilson, D. R., R. N. B. Smith, D. Gregory, C. A. Wilson, A. C. Bushell, and S. Cusack, 2007: The large-scale cloud scheme and saturated specific humidity. Unified Model documentation paper, **29**, Met Office, Exeter, UK.

Wilson, D. R., A. C. Bushell, A. M. Kerr-Munslow, J. D. Price, and C. J. Morcrette, 2008: PC2: A prognostic cloud fraction and condensation scheme. I: Scheme description. *Quart.*

J. Roy. Meteor. Soc., **134**, 2093–2107, doi:10.1002/qj.333.

Winker, D. M., M. A. Vaughan, A. Omar, Y. Hu, K. A. Powell, Z. Liu, W. H. Hunt, and S. A. Young, 2009: Overview of the CALIPSO mission and CALIOP data processing algorithms. *J. Atmos. Ocean. Technol.*, **26**, 2310–2323, https://doi.org/10.1175/2009JTECHA1281.1.

Wood, R., 2012: Stratocumulus clouds. *Mon. Wea. Rev.*, **140**, 2373–2423, doi:10.1175/MWR-D-11-00121.1.

Wood, R., and P. R. Field, 2000: Relationships between total water, condensed water, and cloud fraction in stratiform clouds examined using aircraft data. *J. Atmos. Sci.*, **57**, 1888–1905.

Wood, R., and C. S. Bretherton, 2006: On the relationship between stratiform low cloud cover and lower-tropospheric stability. *J. Climate*, **19**, 6425–6432.

Wood, R., and D. L. Hartmann, 2006: Spatial variability of liquid water path in marine low cloud: The importance of mesoscale cellular convection. *J. Climate*, **19**, 1748–1764.

Wood, R., P. R. Field, and W. R. Cotton, 2002: Autoconversion rate bias in stratiform boundary layer cloud parameterization. *Atmos. Res.*, **65**, 109–128.

Wood, R., and Coauthors, 2011: The VAMOS Ocean-Cloud-Atmosphere-Land Study Regional Experiment (VOCALS-REx): Goals, platforms, and field operations. *Atmos. Chem. Phys.*, **11**, 627–654, doi:10.5194/acp-11-627-2011.

Xu, K. M., and D. A. Randall, 1996: Evaluation of statistically based cloudiness parameterizations used in climate models. *J. Atmos. Sci.*, **53**, 3103–3119.

Yamaguchi, T., and D. A. Randall, 2008: Large-eddy simulation of evaporatively driven entrainment in cloud-topped mixed layers. *J. Atmos. Sci.*, **65**, 1481–1504, doi:10.1175/2007JAS2438.1.

Yukimoto, S., Y. Adachi, M. Hosaka, T. Sakami, H. Yoshi-mura, M. Hirabara, T. Y. Tanaka, E. Shindo, H. Tsujino, M. Deushi, R. Mizuta, S. Yabu, A. Obata, H. Nakano, T. Koshiro, T. Ose, and A. Kitoh, 2012: A new global climate model of the Meteorological Research Institute: MRI-CGCM3—Model description and basic performance—. *J. Meteor. Soc. Japan*, **90A**, 23–64.

Yukimoto, S., H. Kawai, T. Koshiro, N. Oshima, K. Yoshida, S. Urakawa, H. Tsujino, M. Deushi, T. Tanaka, M. Hosaka, S. Yabu, H. Yoshimura, E. Shindo, R. Mizuta, A. Obata, Y. Adachi, and M. Ishii, 2019: The Meteorological Research Institute Earth System Model version 2.0, MRI-ESM2.0: Description and basic evaluation of the physical component. *J. Meteor. Soc. Japan*, **97**, 931–965, doi:10.2151/jmsj.2019-051.

Zelinka, M. D., S. A. Klein, and D. L. Hartmann, 2012a: Computing and partitioning cloud feedbacks using cloud property histograms. Part I: Cloud radiative kernels. *J. Climate*, **25**, 3715–3735, https://doi.org/10.1175/JCLI-D-11-00248.1.

Zelinka, M. D., S. A. Klein, and D. L. Hartmann, 2012b: Computing and partitioning cloud feedbacks using cloud property histograms. Part II: Attribution to changes in cloud amount, altitude, and optical depth. *J. Climate*, **25**, 3736–3754, https://doi.org/10.1175/JCLI-D-11-00249.1.

Zelinka, M. D., S. A. Klein, K. E. Taylor, T. Andrews, M. J. Webb, J. M. Gregory, and P. M. Forster, 2013: Contributions of different cloud types to feedbacks and rapid adjustments in CMIP5. *J. Climate*, **26**, 5007–5027, https://doi.org/10.1175/JCLI-D-12-00555.1.

Zelinka, M. D., T. Andrews, P. M. Forster, and K. E. Taylor, 2014: Quantifying components of aerosol-cloud-radiation interactions in climate models. *J. Geophys. Res. Atmos.*, **119**, 7599–7615, doi:10.1002/2014JD021710.

Zelinka, M. D., T. A. Myers, D. T. McCoy, S. Po‐Chedley, P. M. Caldwell, P. Ceppi, S. A. Klein, and K. E. Taylor, 2020: Causes of higher climate sensitivity in CMIP6 models. *Geophys. Res. Lett.*, **47**, 1–12, https://doi.org/10.1029/2019GL085782.

Zhang, M., and C. Bretherton, 2008: Mechanisms of low cloud–climate feedback in idealized single-column simulations with the Community Atmospheric Model, version 3 (CAM3). *J. Climate*, **21**, 4859–4878.

Zhang, M. H., and Coauthors, 2005: Comparing clouds and their seasonal variations in 10 atmospheric general circulation models with satellite measurements. *J. Geophys. Res. Atmos.*, **110**, D15S02, https://doi.org/10.1029/2004JD005021.

Zhang, M., C. Bretherton, M. Webb, and P. Siebesma, 2010: CFMIP-GCSS Intercomparison of Large Eddy Models and Single Column Models (CGILS). *GEWEX News*, **Vol. 20**, No. 2, May 2010.

Zhang, M., C. S. Bretherton, P. N. Blossey, S. Bony, F. Brient, and J. C. Golaz, 2012: The CGILS experimental design to investigate low cloud feedbacks in general circulation models by using single-column and large-eddy simulation models. *J. Adv. Model. Earth Syst.*, **4**, 1–15, doi:10.1029/2012MS000182.

Zhang, M., and Coauthors, 2013: CGILS: Results from the first phase of an international project to understand the physical mechanisms of low cloud feedbacks in single column models. *J. Adv. Model. Earth Syst.*, **5**, 826–842, doi:10.1002/2013MS000246.

Zhao, M., and Coauthors, 2018: The GFDL Global Atmosphere and Land Model AM4.0/LM4.0: 2. Model description, sensitivity studies, and tuning strategies. *J. Adv. Model. Earth Syst.*, **10**, 735–769, https://doi.org/10.1002/2017MS001209.

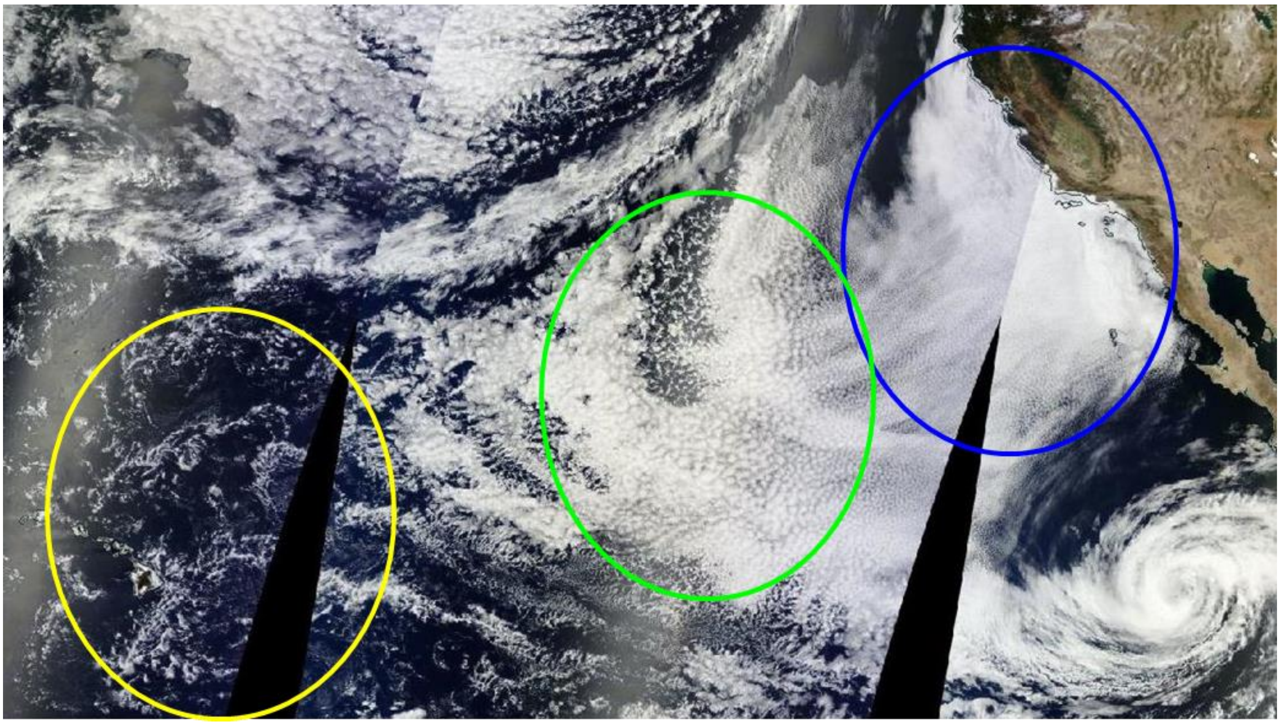

Fig. 1 Visible image of marine low clouds, including stratus (blue circle), stratocumulus (green circle), and cumulus clouds (yellow circle), over an area from off the coast of California to Hawaii, acquired by MODIS on July 1, 2014. Source: NASA Worldview.

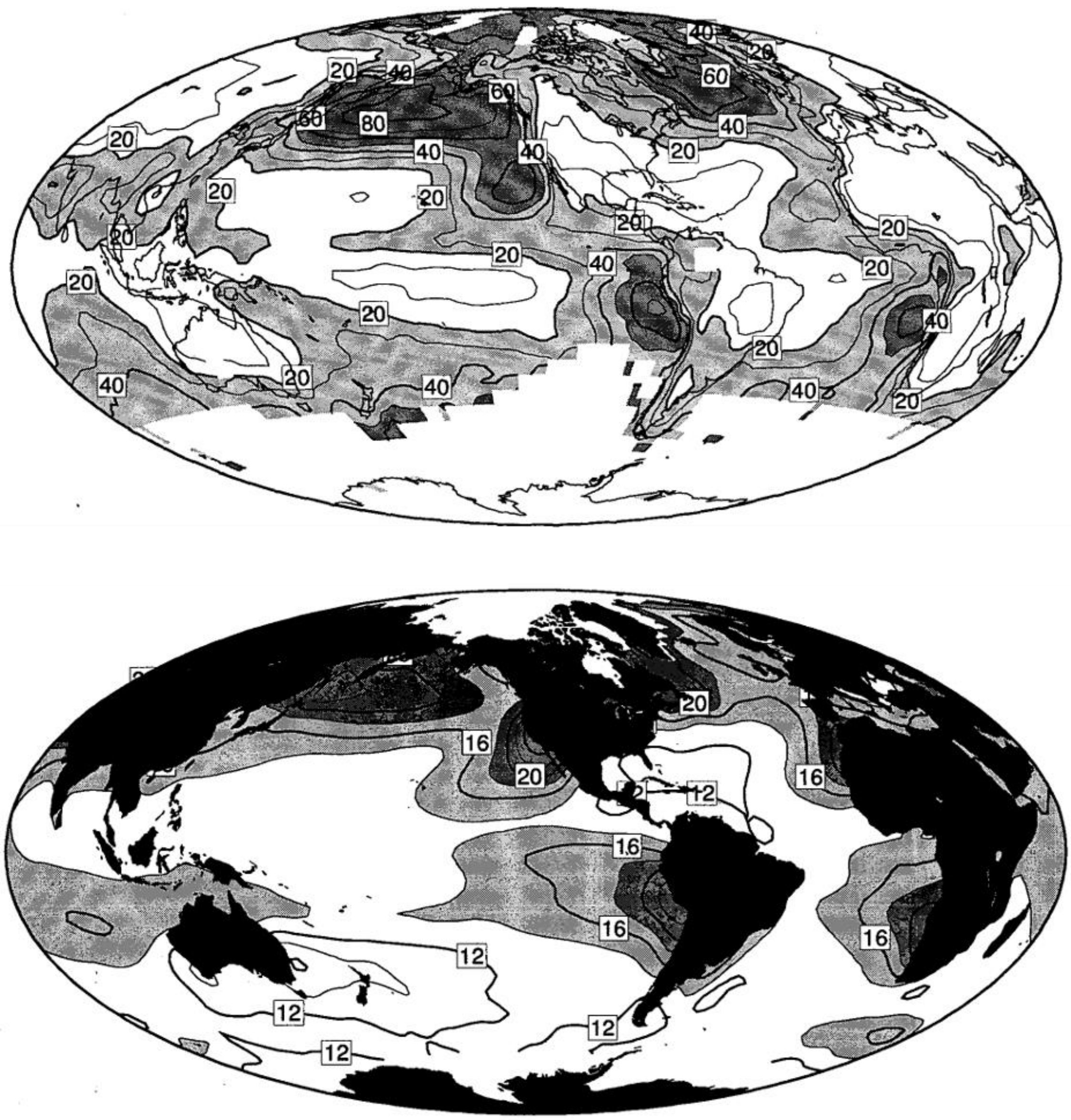

Fig. 2 Upper panel: Climatology (percent) of low stratiform cloud amount, which consists of stratus, stratocumulus, and sky-obscuring fog, as reported by surface-based observers in June, July, and August. Lower panel: Same as the upper panel but for lower tropospheric stability in Kelvin (Klein and Hartmann 1993). © American Meteorological Society. Used with permission.

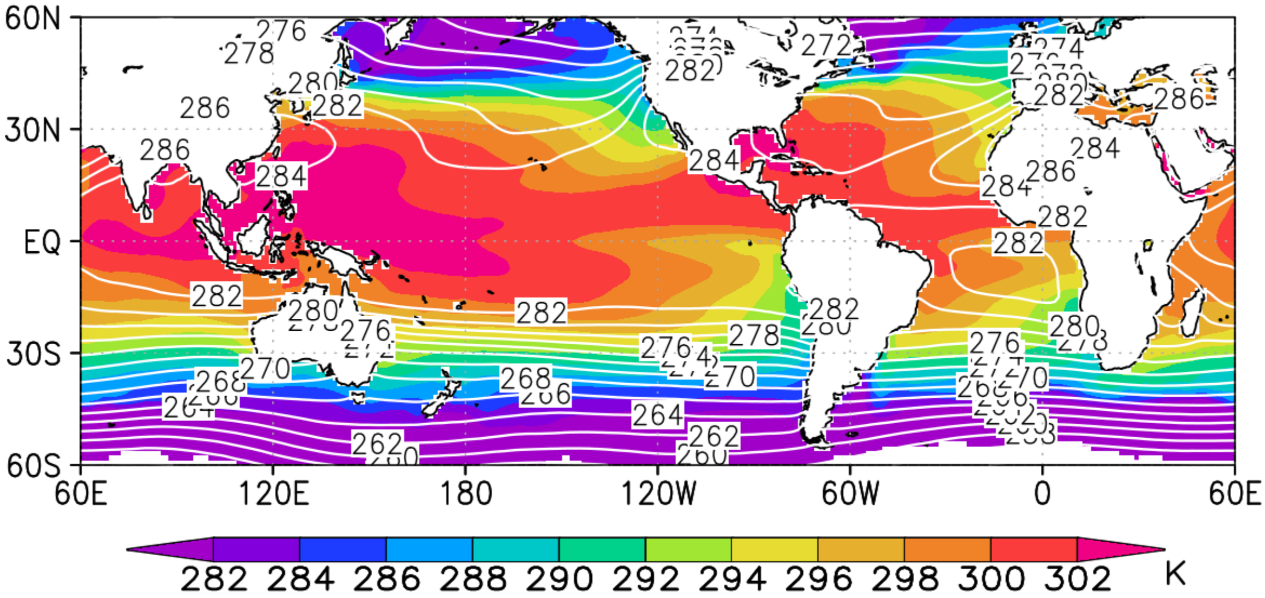

Fig. 3 Climatology of SST (K; shading) and temperature at 700 hPa (K; contours) for July over 1979–2008. The data are from the European Centre for Medium-Range Weather Forecasts (ECMWF) interim reanalysis (ERA-Interim) (Dee et al. 2011).

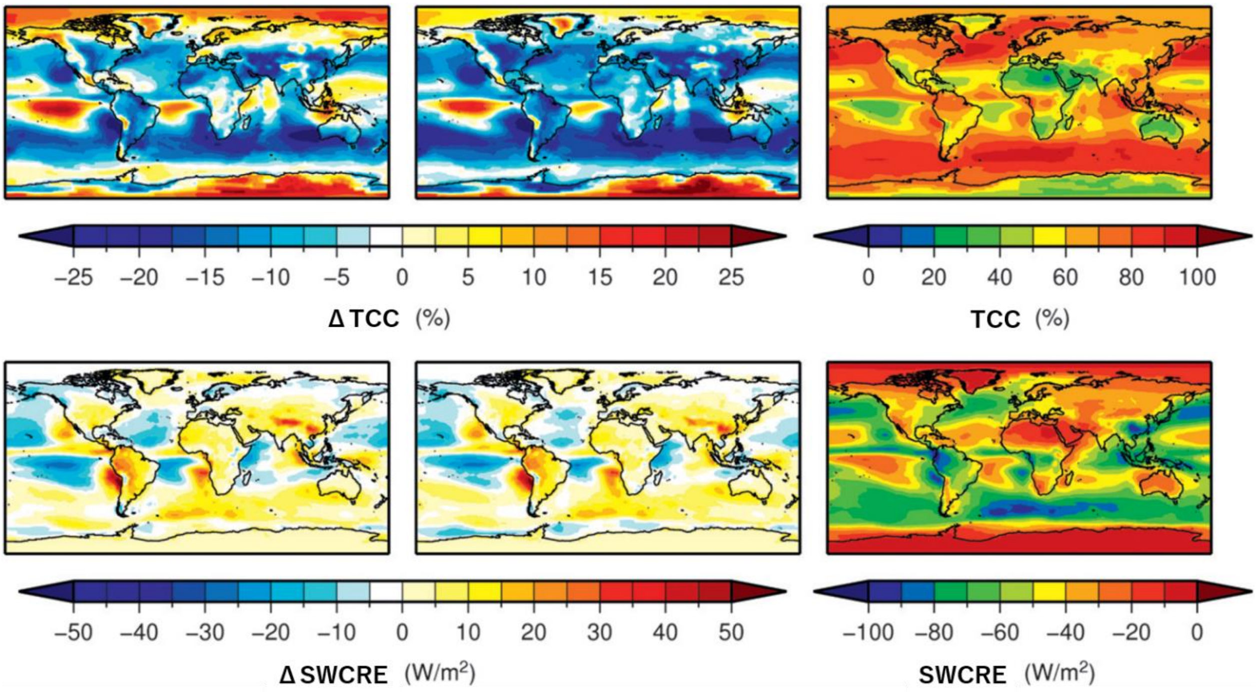

Fig. 4 Biases of (top) total cloud cover and (bottom) shortwave cloud radiative effect for the (left) CMIP3 and (middle) CMIP5 multimodel means with respect to (right) satellite observations. They are averaged over the 20 years 1986–2005. ISCCP data are used as observational data for total cloud cover and ISCCP-FD for the shortwave cloud radiative effect (modified after fig. 2 in Lauer and Hamilton 2013). © American Meteorological Society. Used with permission.

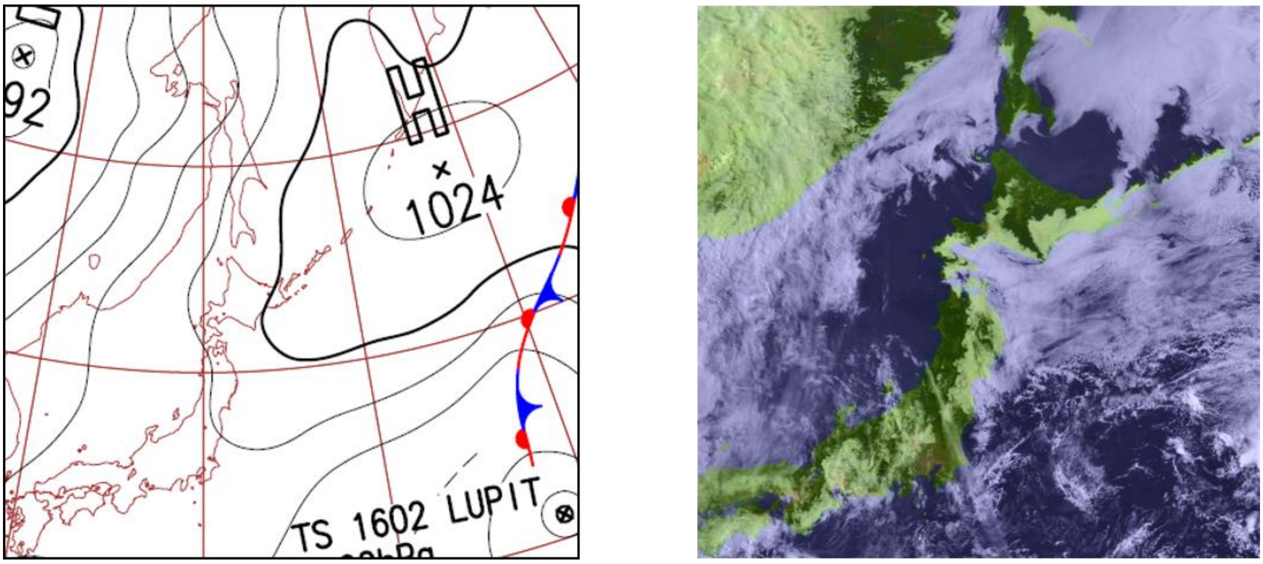

Fig. 5 (left) Surface weather chart and (right) Himawari-8 satellite visible image of a typical Yamase phenomenon at 0900 local time on July 24, 2016. The weather chart is from the JMA and the satellite image is provided by Kochi University (Weather Home), University of Tokyo, and the JMA.

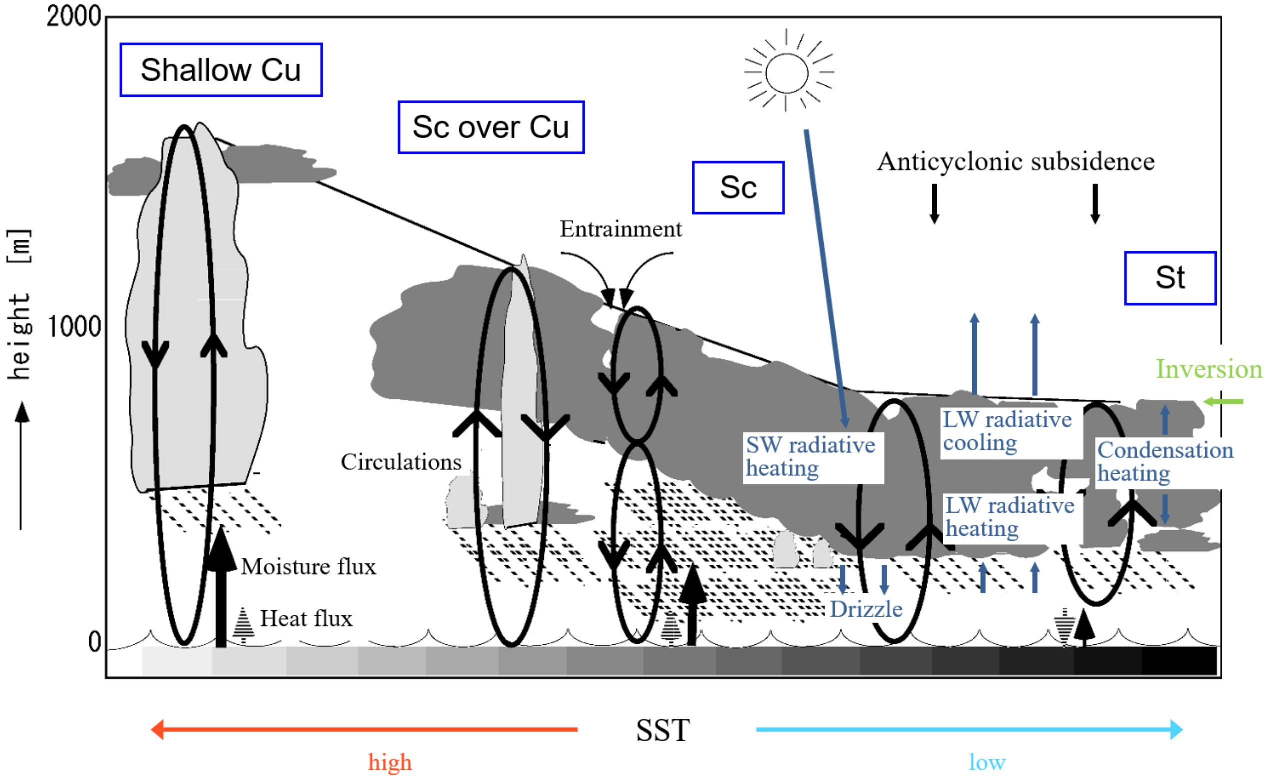

Fig. 6 Schematic of processes related to subtropical low clouds (modified after fig. 2 in de Roode and Duynkerke 1997). Cloud regimes are denoted in blue rectangles: St for stratus, Sc for stratocumulus, and Cu for cumulus. © American Meteorological Society. Used with permission.

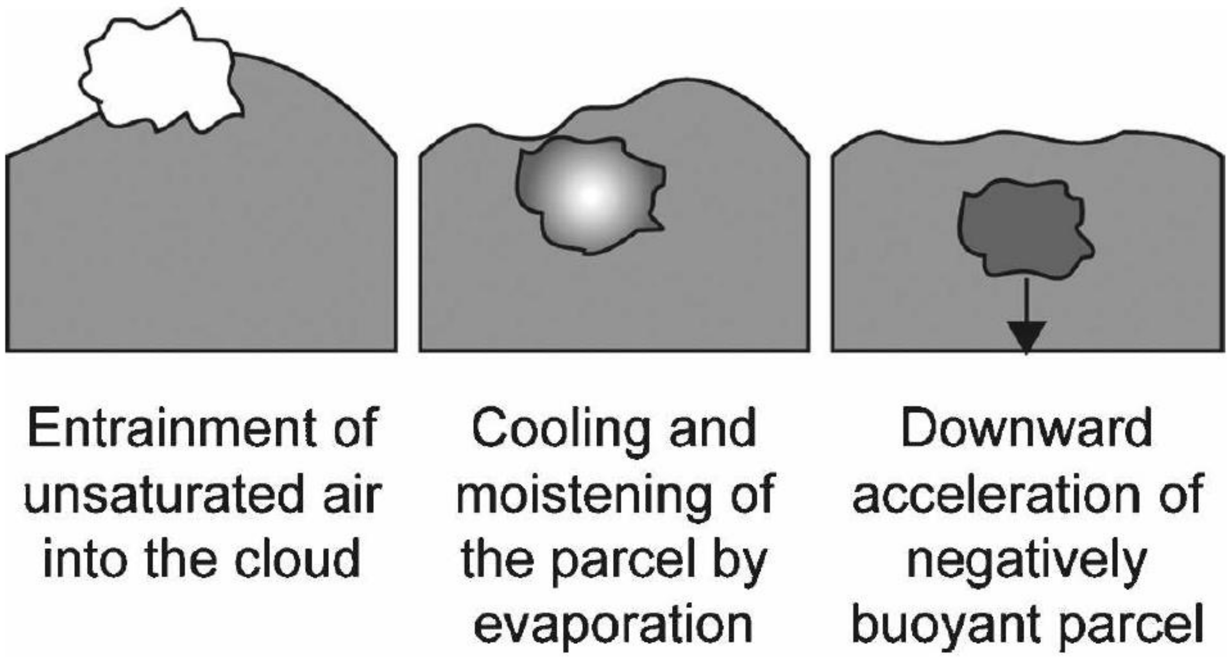

Fig. 7 Schematic of cloud top entrainment. The shaded area represents cloudy air (fig. 1 in Yamaguchi and Randall 2008, after Randall 1980). © American Meteorological Society. Used with permission.

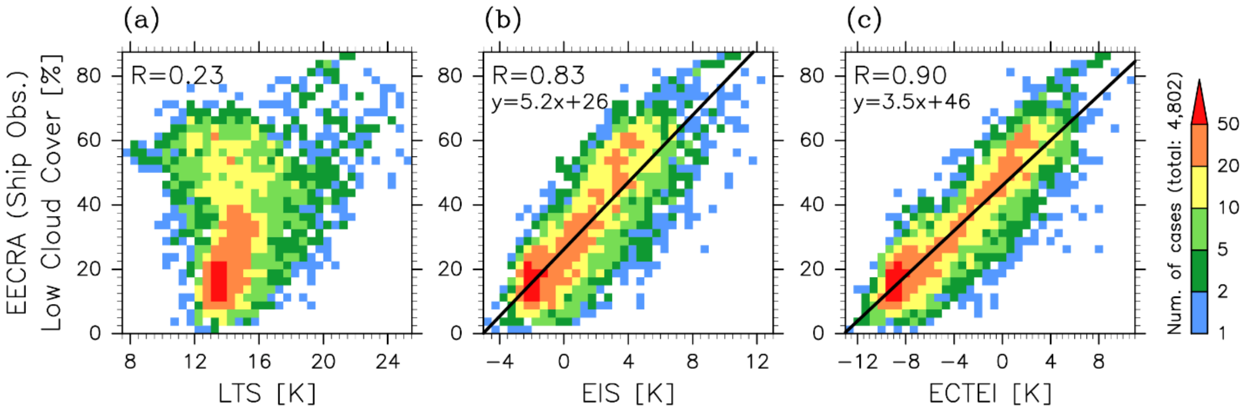

Fig. 8 Frequencies of occurrence of low stratiform cloud cover (combined cloud cover of stratocumulus, stratus, and sky-obscuring fog) sorted by (a) LTS, (b) EIS, and (c) ECTEI (β = 0.23), based on all 5° × 5° seasonal climatology data. Cloud cover data were obtained from the extended edited cloud report archive (EECRA; Hahn and Warren, 2009) shipboard observations. Stability indexes were calculated using the ECMWF 40-year Re-Analysis (ERA-40) data (Uppala et al. 2005) (1957–2002). All the data between 60°N and 60°S for all seasons were used. Linear regression lines and the correlation coefficients are shown. From Kawai et al. (2019).

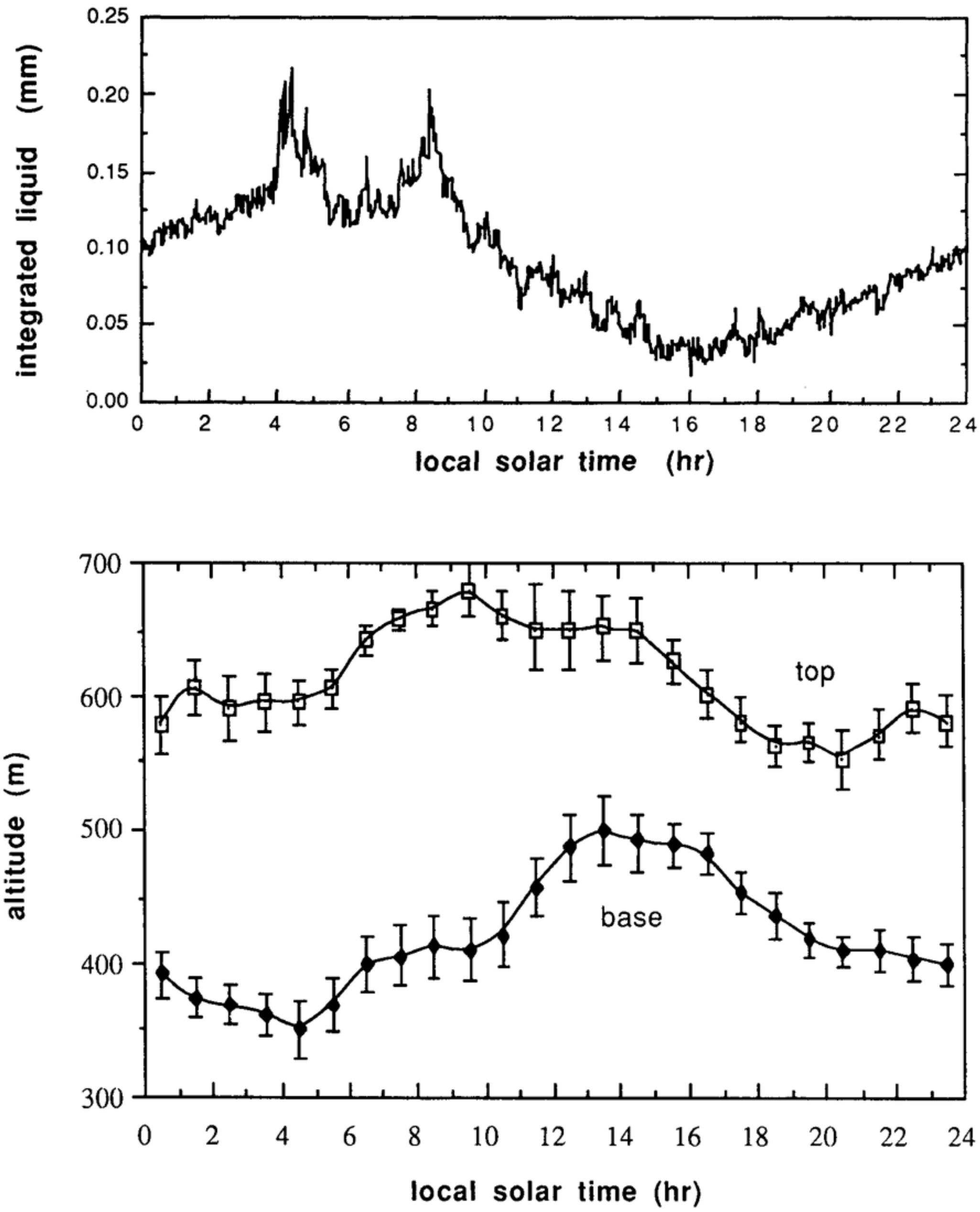

Fig. 9 Diurnal variations in (top) liquid water path and (bottom) cloud-top and cloud-base heights observed off the coast of California in FIRE (First ISCCP Regional Experiment) during July 1987 (fig. 2 and fig. 4 in Blaskovic et al. 1991). © American Meteorological Society. Used with permission.

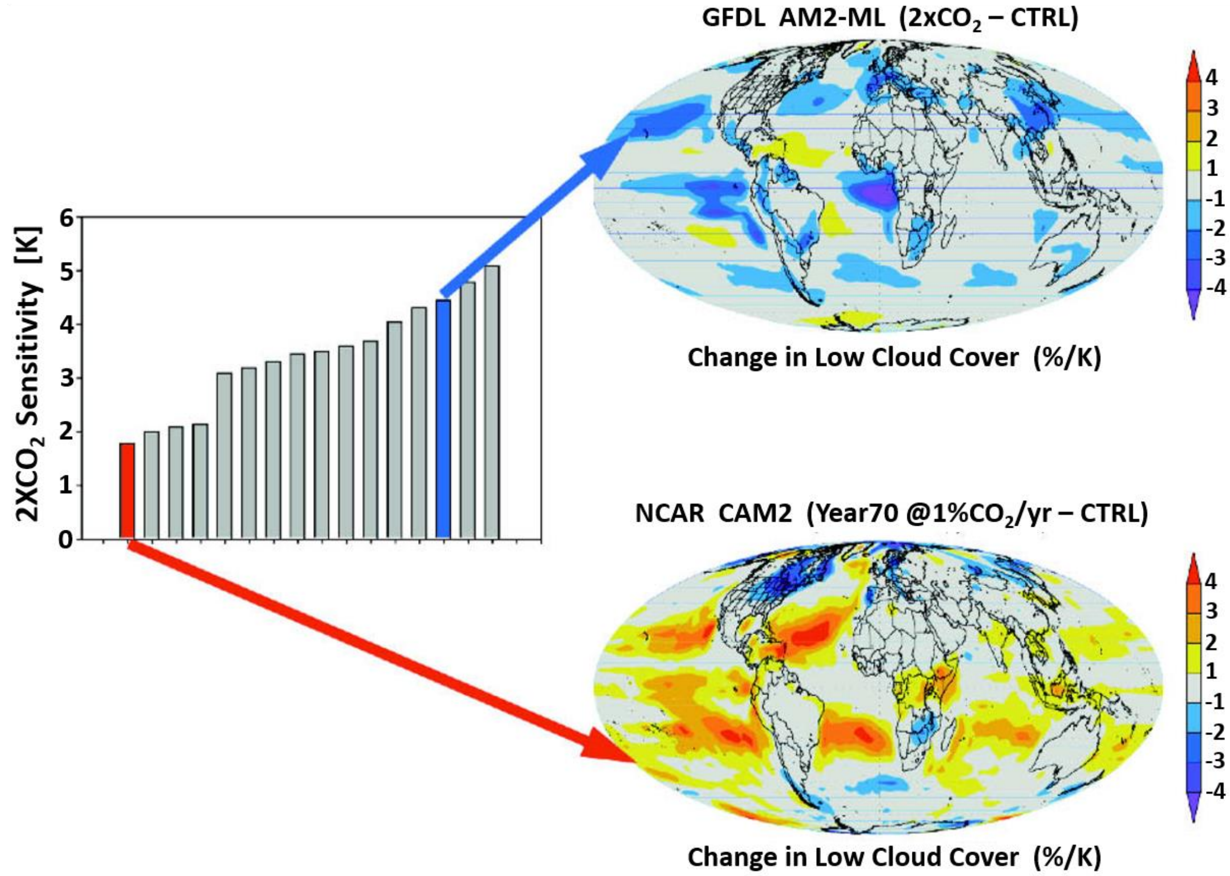

Fig. 10 (left) Surface warming estimates in doubled CO_2 climates from climate models developed for CMIP3. Simulation data forced by a 1% yr^{-1} increase in CO_2 are used. Shown is the difference of the 20-yr average of the simulation with present (1961–80) and increasing CO_2 (corresponding broadly to a time of doubled CO_2 concentrations). (right) The changes in low cloud cover averaged over this same period for two models that fall on either end of the projected warming range (modified after fig. 1 in Stephens 2005). © American Meteorological Society. Used with permission.

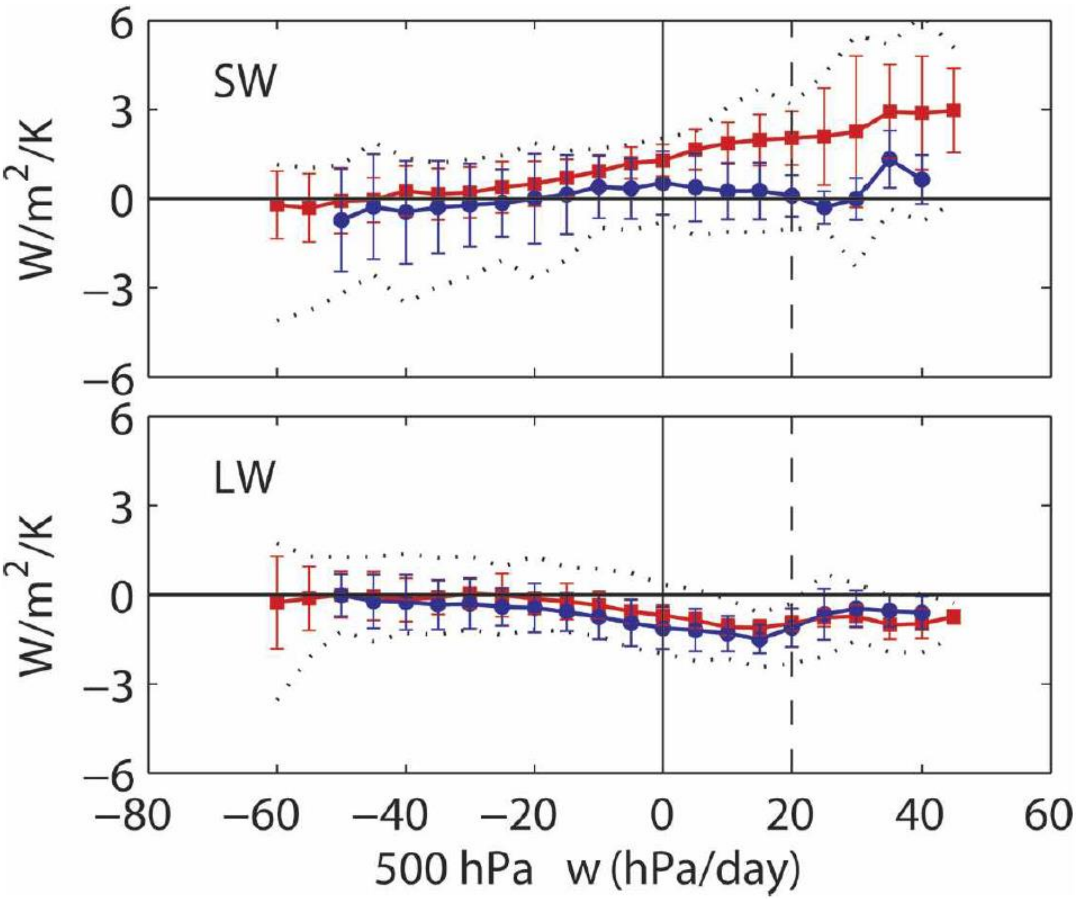

Fig. 11 Sensitivity (W m^{-2} K^{-1}) of the tropical (30°S–30°N) shortwave and longwave cloud radiative effect to changes in SST associated with climate change (in a scenario in which the CO_2 increases by 1% yr^{-1}) derived from 15 coupled ocean–atmosphere GCMs participating in the AR4. The sensitivity is computed for different large-scale atmospheric circulation regimes (the 500-hPa large-scale vertical pressure velocity is used as a proxy for large-scale motion). Results are presented for two groups of GCMs: models that predict a positive anomaly in the tropically averaged net cloud radiative effect in climate change (red; eight models) and models that predict a negative anomaly (blue; seven models) (fig. 9 in Bony et al. 2006, after Bony and Dufresne 2005). © American Geophysical Union.

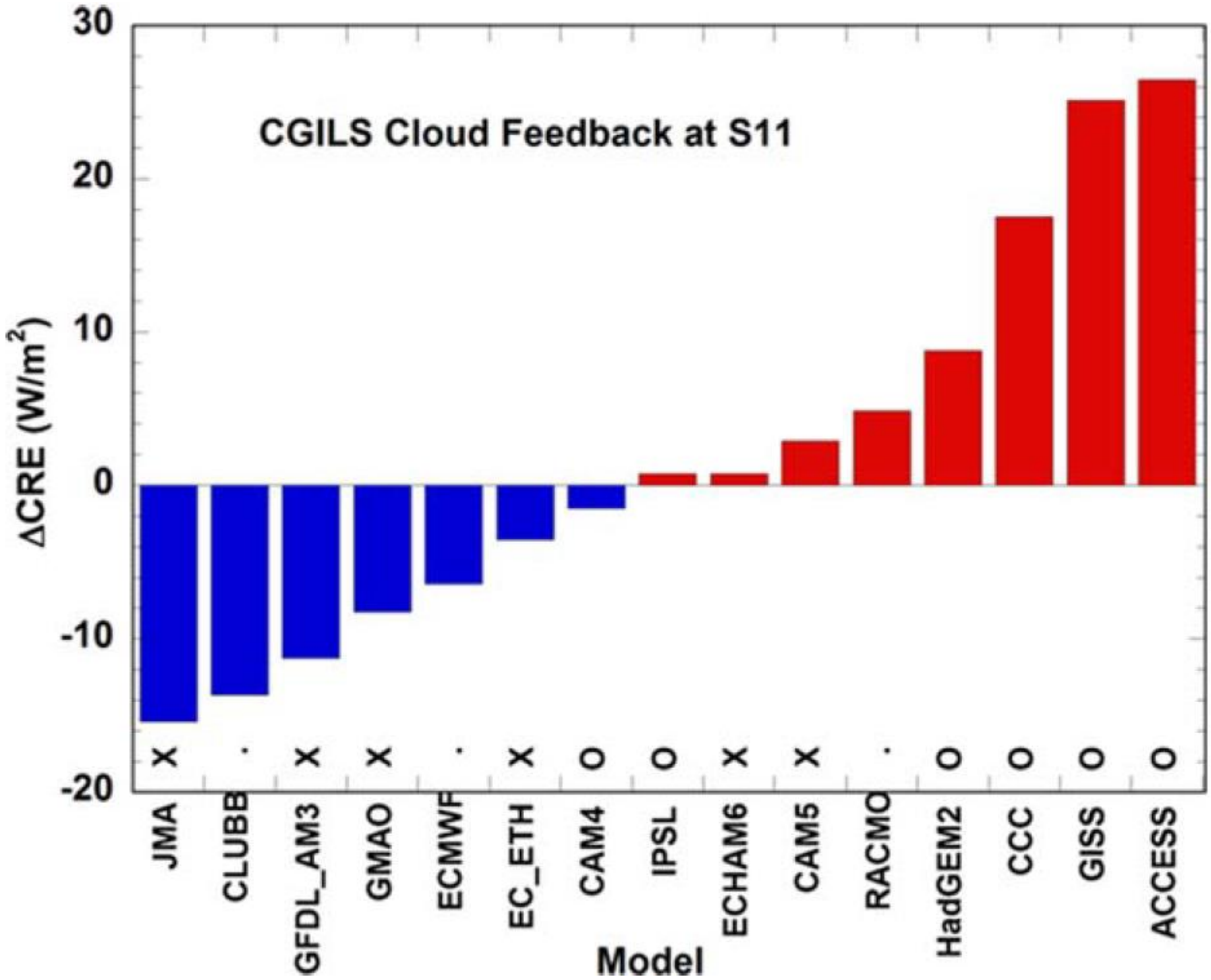

Fig. 12 Change in cloud radiative effect (CRE, W m^{-2}) in SCMs for stratocumulus (at location S11 in CGILS: 32ºN, 129ºW) corresponding to a 2 K SST perturbation. The 'X' above a model name indicates that the shallow convection scheme is not active; 'O' indicates that the shallow convection scheme is active. Models without these characters either do not separately parameterize shallow convection and atmospheric boundary layer turbulence, or do not submit results with information on convection (fig. 7 in Zhang et al. 2013). © American Geophysical Union.

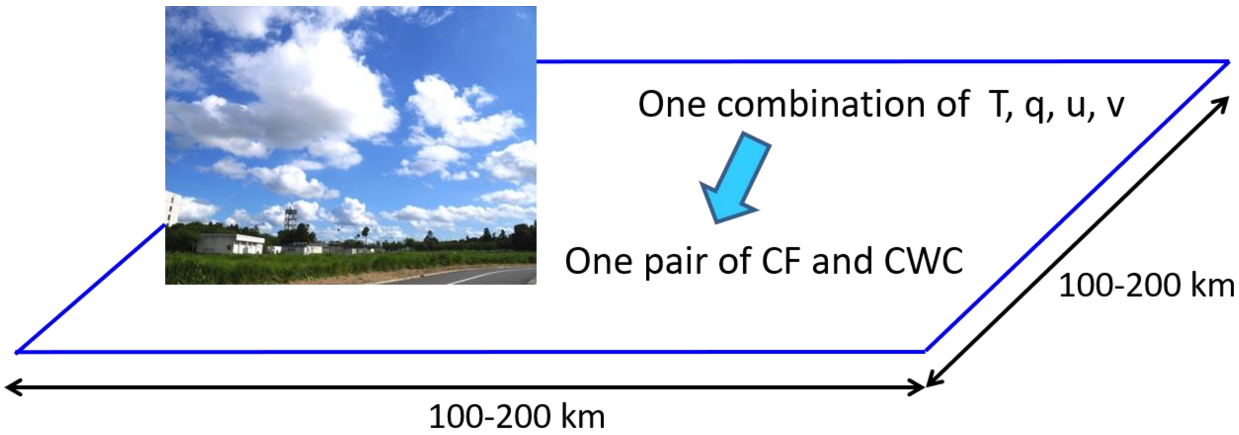

Fig. 13 Schematic of a GCM grid surrounding a photograph of real clouds. One pair of cloud fraction (CF) and cloud water content (CWC) values is determined from a combination of prognostic variables in the GCM; e.g., temperature (*T*), humidity (*q*), and wind (*u*, *v*), which do not have subgrid fluctuation information. The photograph of the clouds was taken in Tsukuba on July 24, 2016 (courtesy of Osamu Arakawa).

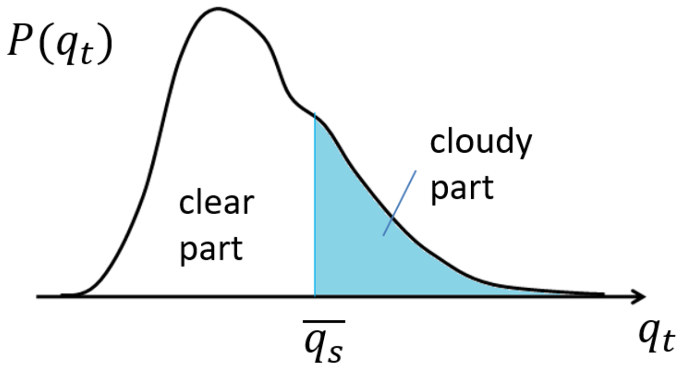

$$A = \int_{\overline{q_s}}^{\infty} P(q_t)\,dq_t$$

$$\overline{q_c} = \int_{\overline{q_s}}^{\infty} (q_t - \overline{q_s})P(q_t)\,dq_t$$

Fig. 14 Schematic of PDF-based cloud schemes. *P* is the probability density function of the total water content, normalized to 1. Cloud fraction and cloud water content are calculated using the equations to the right. Overbars denote the spatial average in each model grid box.

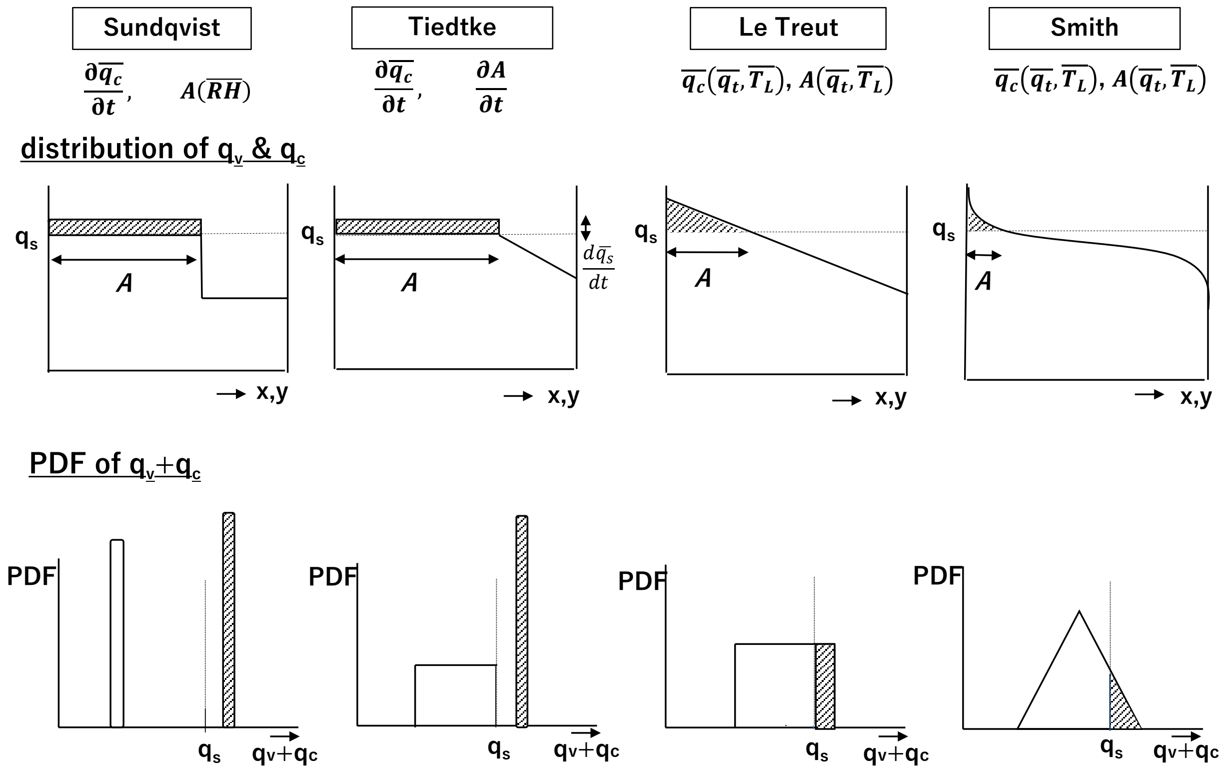

Fig. 15 (Top panels) Distributions of specific humidity and cloud water content in a grid box for various cloud schemes. Hatching corresponds to cloud water content. (Bottom panels) The corresponding probability density functions of the total water content (specific humidity + cloud water content). Hatching denotes cloudy parts and the area of hatching corresponds to cloud fraction.

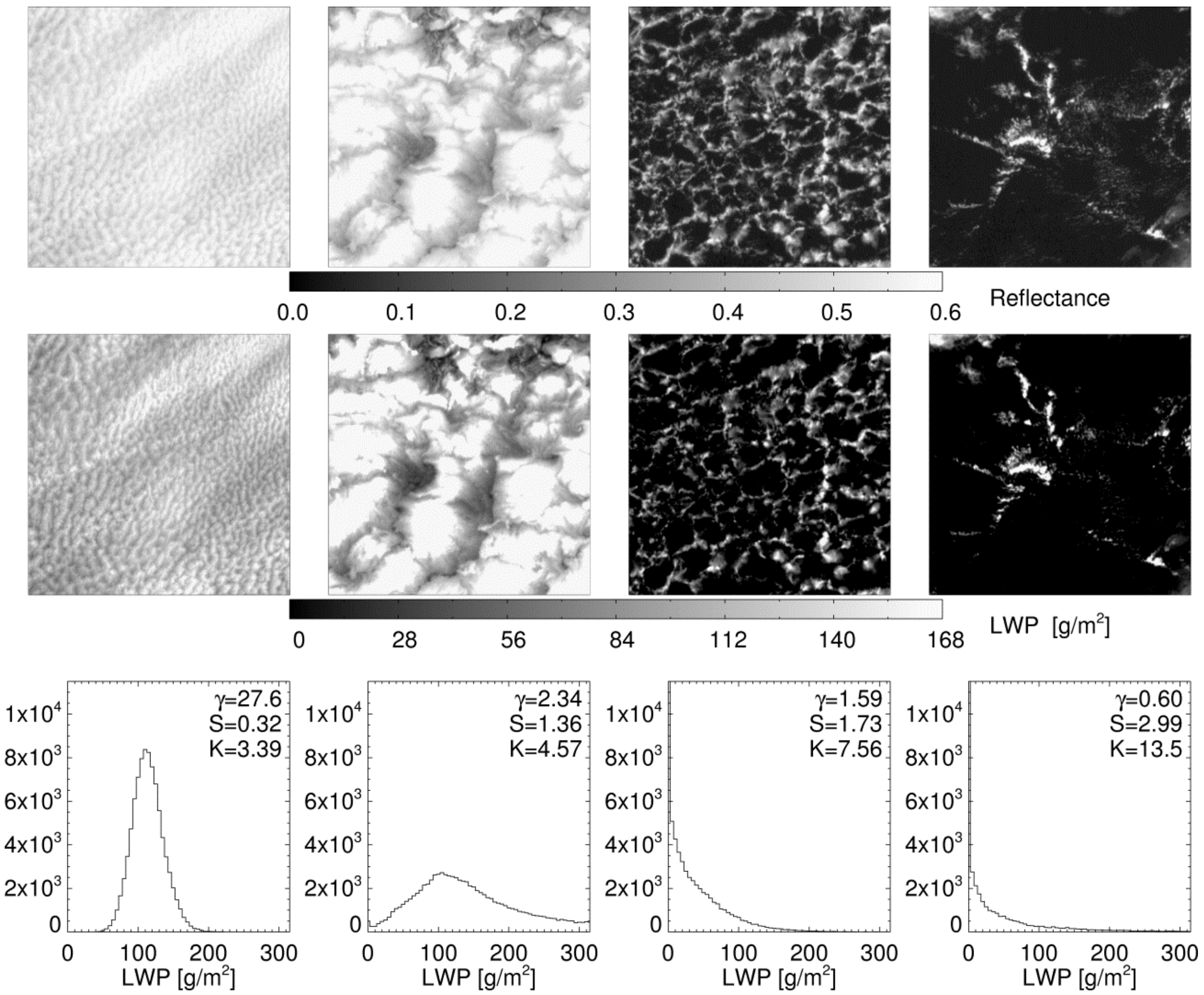

Fig. 16 Examples of images, from distinct cloud regimes, of (top) reflectance, (middle) LWP (g m^{-2}), and (bottom) PDFs of LWP. The areas correspond to 200 km × 200 km and the reflectance is calculated from Geostationary Operations Environmental Satellite (GOES) visible data. Values of homogeneity (γ), skewness (S), and kurtosis (K) for each PDF are indicated in lower panels. Fig. 3 in Kawai and Teixeira 2010. © American Meteorological Society. Used with permission.

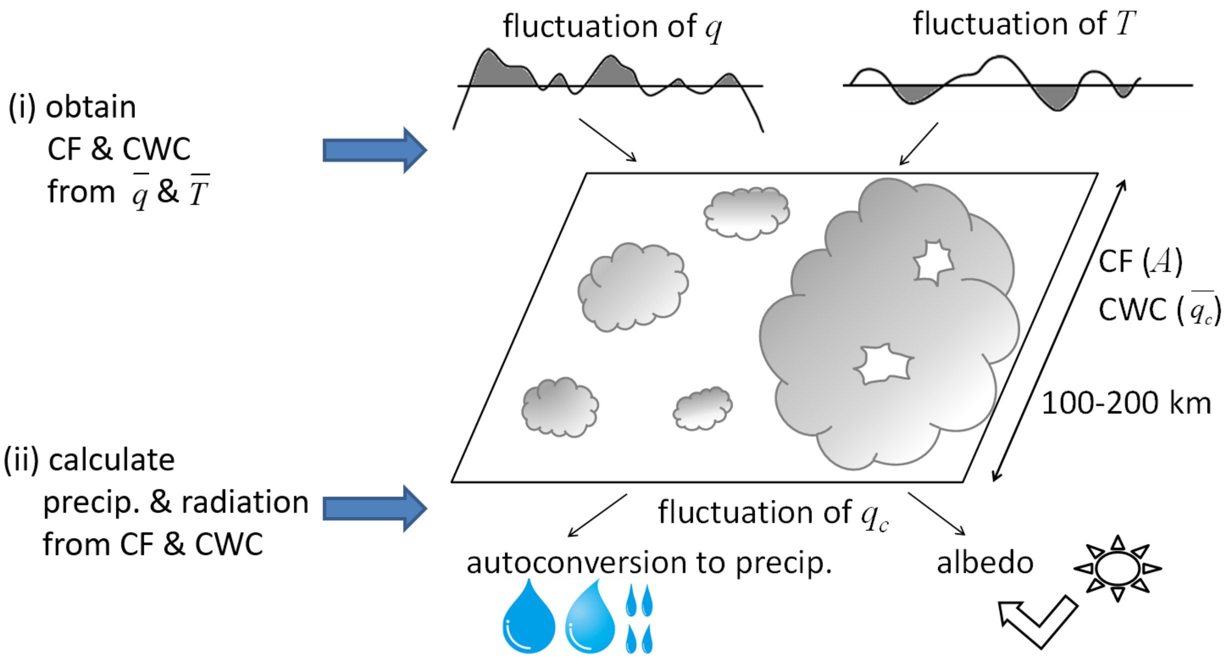

Fig. 17 Schematic of two steps that require subgrid PDF information related to cloud schemes for atmospheric model calculations. The first step is to determine a pair of cloud fraction and cloud water content values from humidity and temperature. The second step is to calculate the autoconversion rate of cloud water to precipitation in the moist processes and albedo in the radiation processes, from cloud fraction and cloud water content. These are affected by the inhomogeneity of cloud water content in the model grid box.

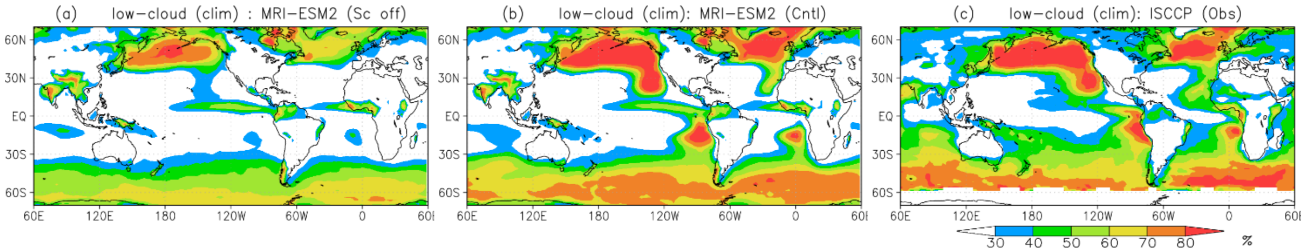

Fig. 18 Low cloud cover (below 680 hPa) in July in units of [%]. Output from the atmospheric model of MRI-ESM2 for 2000–2014 under given SST: (a) a version with the stratocumulus scheme off and (b) a control version. (c) ISCCP observational data for 1986–2005 where the low cloud cover is corrected under an assumption of random cloud overlap.

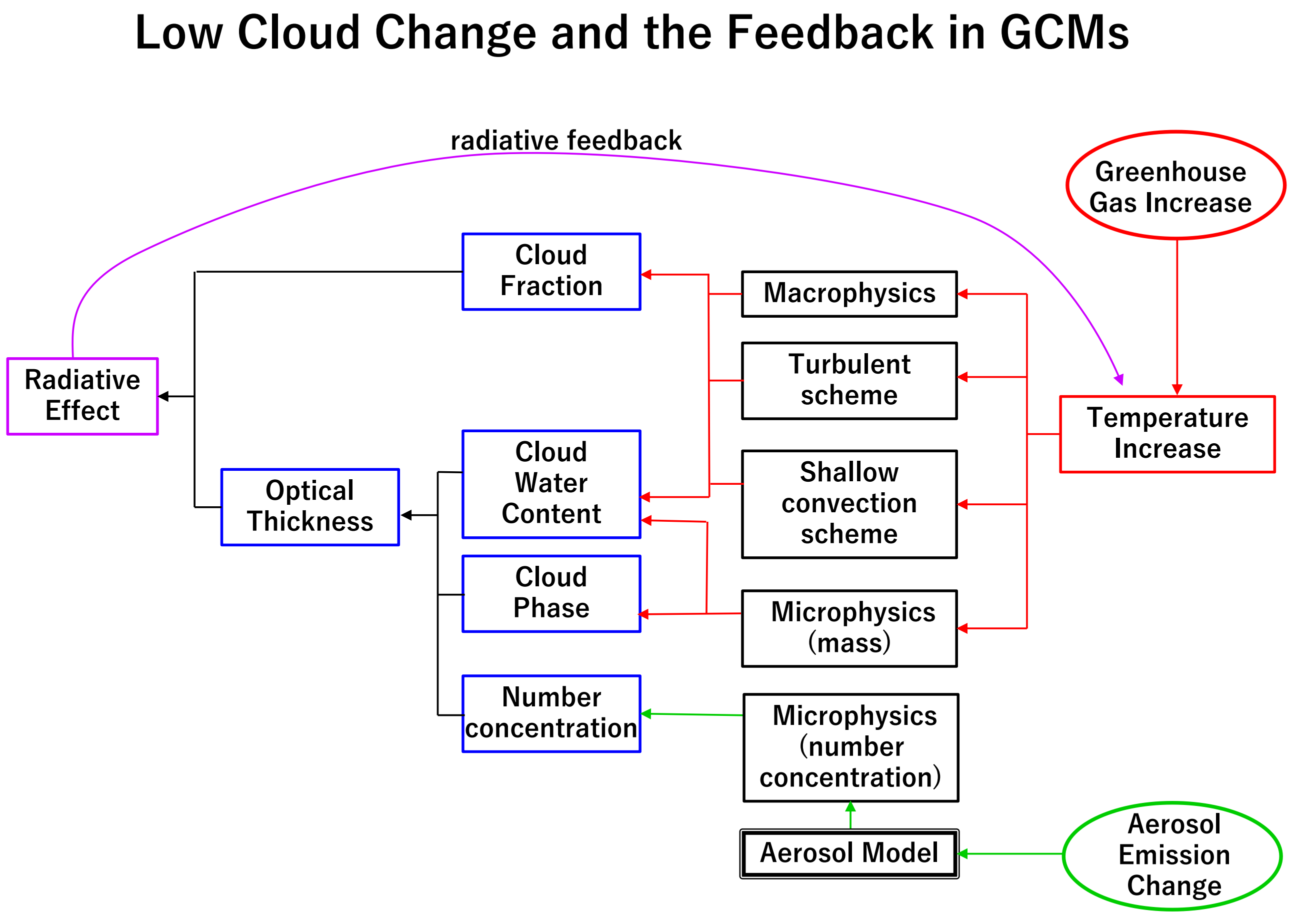

Fig. 19 Schematic diagram of low cloud changes and related physical processes in GCMs in climate simulations. Ovals show forcing given in climate simulations. Cloud properties (blue boxes) that are affected by the forcing and physical processes (black boxes) that mainly affect the cloud properties are shown. The connections between boxes are major routes, although there are other minor relationships between them. Red lines show changes or effects related to greenhouse gas forcing and green lines to aerosol emission forcing.

Table 1 List of major field campaigns associated with MLCs. Sc denotes stratocumulus and Cu denotes cumulus. Abbreviations are as follows: BOMEX (the Barbados Oceanographic and Meteorological Experiment), DYCOMS-II (the Second Dynamics and Chemistry of Marine Stratocumulus), and RICO (the Rain in Cumulus over the Ocean). See text for other abbreviations.

Field campaigns	**Year**	**Area**	**Main target**	**Reference**
BOMEX	May-Jul 1969	Trop. Atlantic	Cu	Davidson (1968)
FIRE	Jun & Jul 1987	off California	Sc	Albrecht et al. (1988)
ASTEX	Jun 1992	NE Atlantic	Sc & Cu	Albrecht et al. (1995)
DYCOMS-II	Jul 2001	off California	Sc	Stevens et al. (2003)
EPIC	Sep & Oct 2001	off Peru	Sc	Bretherton et al. (2004b)
RICO	Nov 2004-Jan 2005	Trop. Atlantic	Cu	Rauber et al. (2007)
VOCALS-REx	Oct & Nov 2008	off Peru	Sc	Wood et al. (2011)
EUREC^{4}A	Jan & Feb 2020	Trop. Atlantic	Cu	Bony et al. (2017)

Table 2 List of experiments using atmospheric components of climate models in CMIP5. Strings of letters show the names of experiments commonly used in the project. The sign '−' denotes experiments not proposed. The name 'aqua' denotes an aqua planet experiment, where zonally uniform SST is given for an ocean-covered earth. The name 'sstClim' denotes an experiment where SST climatology of pre-industrial control and preindustrial aerosols including sulfate are given. The CO_2 concentration is not changed for SST+4K experiments (both uniform and patterned SST perturbation), and SST is not changed for quadrupled CO_2 experiments.

Basic experim.	**SST+4K uniform**	**SST+4K patterned**	**Quadrupled CO2**	**All aerosols of year 2000**	**Only sulfate of year 2000**
amip	amip4K	amipFuture	amip4xCO2	−	−
aqua	aqua4K	−	aqua4xCO2	−	−
sstClim	−	−	sstClim4xCO2	sstClimAerosol	sstClimSulfate